Noise Analysis of an Ultra Wide Band FMCW Ranging Receiver

THESIS

submitted in partial fulfillment of the
requirements for the degree of

MASTER OF SCIENCE
in
ELECTRICAL ENGINEERING

by

Alexander David Visser
Student number 1339095
born in Beverwijk, The Netherlands

Public Defense
on
5 July 2010

Wireless Mobile Communications
Department of Telecommunications
Faculty of Electrical Engineering, Mathematics and Computer Science
Delft University of Technology

TU Delft
Delft University of Technology

Thesis supervisor: Dr. ir. G.J.M. Janssen

Thesis Committee Members :

Advisor:	Dr.ir. G.J.M. Janssen, WMC EEMCS TU Delft
Chairperson:	Prof.dr.ir. I.G.M.M. Niemegeers, WMC EEMCS TU Delft
Member:	Dr.ir. H. Nikookar, MT EEMCS TU Delft

Abstract

This thesis, analyses the performance of an Ultra Wide Band (UWB) Frequency Modulated Continuous Wave (FMCW) ranging system in the presence of additive white Gaussian noise (AWGN). The distortion of the UWB FMCW signal's phase, due to noise, deteriorates its frequency spectrum components. This corrupts the multipath delay information and therefore the range information.

The Auto Correlation Function (ACF) shows that the receiver's output noise is stationary. Together with the statistical properties it describes the receiver's output noise process. This noise process has a complex valued Gaussian frequency spectrum and is not white anymore.

The maximum range of the UWB FMCW receiver system is proportional to the bandwidth of the UWB FMCW signal and inversely proportional to the SNR. Compared to an UWB pulse based ranging system, with equal input parameters, the UWB FMCW ranging system has a higher maximum range, because an UWB FMCW echo contains more energy than an UWB pulse echo.

The presence of noise causes frequency estimation errors to occur which lead to range errors. The CRLB, which provides a theoretical minimum range error deviation, is inversely proportional to the SNR. For high enough SNR values, simulation shows that the range error deviation is close to the CRLB, resulting in range error deviations in the order of centimeters. Therefore, ranging based on FMCW signal in an indoor environment, is an accurate ranging method.

Table of Contents

List of Abbreviations

ACF	Auto Correlation Function
AoA	Angle of Arrival
AWGN	Additive White Gaussian Noise
BPF	Band Pass Filter
CRLB	Cramer Rao Lower Bound
dB	Decibel
DGPS	Differential Global Positioning System
EIRP	Effective Isotropic Radiated Power
FCC	Federal Communications Commission
FFT	Fast Fourier Transform
FMCW	Frequency Modulated Continuous Wave
GPS	Global Positioning System
GSM	Global System for Mobile communication
ISI	Inter Symbol Interference
LNA	Low Noise Amplifier
LPF	Low Pass Filter
LOS	Line of Sight
LTI	Linear Time Invariant
MLE	Maximum Likelihood Estimation
NBI	Narrow Band Interference
NF	Noise Figure
NLOS	Non Line of Sight
PDP	Power Delay Profile
PSD	Power Spectral Density
RADAR	Radio Detection and Ranging
RF	Radio Frequency
RMS	Root Mean Square
RSS	Received Signal Strength
Rx	Received/receiver

SNR	Signal to Noise Ratio
SRF	Sweep Repetition Frequency
SRP	Sweep Repetition Period
TDoA	Time Difference of Arrival
ToA	Time of Arrival
Tx	Transmitted/transmitter
UMTS	Universal Mobile Communication System
UWB	Ultra Wide Band
WMC	Wireless Mobile Communication

List of Symbols

A	Signal amplitude
A_r	Received signal amplitude
A_t	Transmitted signal amplitude
a	Attenuation factor
B	Bandwidth
B_{LPF}	Bandwidth of the LPF
B_{BPF}	Bandwidth of the BPF
B_{FMCW}	Bandwidth of the FMCW signal
B_f	Fractional bandwidth
B_R	Resolution bandwidth
$B_S(f)$	Output of FFT, Fourier transform of beat signal $b_s(t)$
$B_{s\_FMCW}(f)$	FFT of beat signal without the presence of noise
$B_{s\_noise}(f)$	FFT of beat signal only based on noise
$B_{S_x}(f)$	Real frequency components of $B_S(f)$
$B_{S_y}(f)$	Imaginary frequency components of $B_S(f)$
$B_{x\_FMCW}(f)$	Real frequency components of $B_{s\_FMCW}(f)$
$B_{y\_FMCW}(f)$	Imaginary frequency components of $B_{s\_FMCW}(f)$
$B_{x\_noise}(f)$	Real frequency components of $B_{s\_noise}(f)$
$B_{y\_noise}(f)$	Imaginary frequency components of $B_{s\_noise}(f)$
$b_s(t)$	LPF output, beat signal
$b_{s\_noise}(t)$	LPF output only based on noise process
$b_{s\_FMCW}(t)$	LPF output, beat signal without the presence of noise
$b_s[n]$	Time discrete signal of $b_s(t)$
c	Speed of light

d	Distance
d_0	Reference distance
F	Noise figure
f	Frequency
$f(d)$	Distribution function of d
$f(t)$	Time dependent frequency function
f_b	Beat frequency
$\hat{f}_b$	Estimated beat frequency
$f_{b_{\max}}$	Maximum beat frequency
f_c	Centre frequency
f_{co}	Cut off frequency of the LPF
f_h	Highest frequency
f_l	Lowest frequency
f_{sample}	Sampling frequency
f_0	Reference frequency
Δf	Small part of frequency spectrum
G_{fs}	Free space gain
G_r	Receiver antenna gain
G_{SNR}	Ratio between SNR_{LPF} and SNR_{BPF}
G_t	Transmit antenna gain
$h(t)$	Wireless channel impulse response
$h_{BPF}(t)$	Impulse response of the BPF
$h_{LPF}(t)$	Impulse response of the LPF
$H(f,d)$	Transfer function
i	Index number
$L(d_0)$	Constant $\left(\frac{\lambda}{4\pi d_0}\right)^2$
k	Boltzmann's constant

$L(d)$	Distance dependent propagation loss
$L(d_0)$	Free space loss (only related to reference distance)
$L(f,d)$	Distance and frequency dependent propagation loss
$L(f_0,d_0)$	Free space loss
l	Number of clusters
N	Number of multipath components
N_0	The single sided $PSD_n(f)$
n	Index number
n_s	Number of samples
$n(t)$	AWGN signal
M	Number of samples (Matlab simulation)
m	Index number of Nakagami distribution
P	Power
$P_{average}$	Average power
P_{EIRP}	Effective Isotropic Radiated Power
$P_{r_{b_s(t)}}$	Power of signal $b_s(t)$
P_n	Thermal noise power
$P_{n_{FFT}}$	Thermal noise power at the output of the FFT
$P_{n_{b_s(t)}}$	Thermal noise power at the output of the LPF
P_r	Received power
$P_{r_{FFT}}$	Power of the signal at the output of the FFT
P_t	Transmitted power
$P_{t_{MAX}}$	Maximum transmit power
$p(f)$	Rayleigh Distribution function of AWGN $BS(f)$
$p(\psi)$	Distribution function of ψ
$p(\tau_n)$	Received power of n^{th} multipath component
$PSD_n(f)$	Power Spectral Density of $n(t)$
$q(t)$	BPF output signal
R	Distance

$\hat{R}$	Estimated distance
$R_x(t_1, t_2)$	Auto Correlation Function
$r(t)$	Received UWB FMCW signal
SNR_{FFT}	SNR after the FFT unit
SNR_{in}	SNR just before LPF
SNR_{LPF}	SNR just after LPF
SNR_{BPF}	SNR just after BPF
$S(f)$	Fourier transform of $s(t)$
$s(t)$	Transmitted UWB FMCW signal
$s'(t)$	Replica of $s(t)$
T	Signal period
T_0	Noise temperature at room temperature
T_{co}	Cut off period of the LPF
T_{RX}	Noise temperature of a Communication System
T_l	Arrival time of the l^{th} cluster
T_s	Symbol period
T_{sample}	Sample period
T_{system}	Noise temperature of UWB FMCW receiver
T_{sweep}	Signal sweep duration
t	Time
$2W_b$	Bandwidth of the BPF
W_l	Bandwidth of the LPF
w[n]	Weighting factor of the window
x_0	x coordinate of the location of the object of interest
x_i	x coordinate of the location of a receiving antenna
y_0	y coordinate of the location of the object of interest
y_i	y coordinate of the location of a receiving antenna
$z(t)$	Output signal of the multiplier operation

α	Arrival rate of the clusters
β	Arrival rate of the multipath components
β_{ebw}	Effective signal bandwidth
$\Gamma(m)$	Gamma function
Γ	Cluster time decay constant
γ	Multipath time decay constant
$\delta(t)$	Dirac delta function
ζ	Rate of frequency change
η	Path loss exponent
θ	Phase
$\theta_{n,l}$	Phase of n^{th} multipath component from l^{th} cluster
κ	Frequency dependent decaying factor
λ	Wavelength
μ	Mean value
$\mu_{\psi(\text{dB})}$	Mean value of ψ in dB
σ	Standard deviation
σ_{b_s}	Standard deviation of $b_s(t)$
σ_{B_S}	Standard deviation of $B_S(f)$
$\sigma_{\psi(\text{dB})}$	Standard deviation of ψ in dB
τ	Time delay or time difference between two measurements
$\bar{\tau}$	Mean time delay
$\overline{\tau^2}$	Second moment of τ
τ_d	The one-way travel time (delay time)
$\tau_{\max}$	Maximum propagation delay time
$\tau_{n,l}$	Delay time of n^{th} multipath component
$\tau_{n,l}$	Delay time of n^{th} multipath component from l^{th} cluster
τ_{rms}	RMS delay spread
$\phi(t)$	Phase of UWB FMCW signal
ϕ_0	Initial phase at time $t = 0$

ψ	P_t to P_r ratio
$\psi_{(\mathrm{dB})}$	P_t to P_r ratio in dB
Ω	Second moment of random variable r related to Nakagami

List of Figures

List of Tables

Acknowledgements

I would like to thank Dr. ir. Gerard Janssen for giving me the opportunity to work on my Master's thesis at the WMC Group (Wireless Mobile Communication), Department Telecommunications of the Faculty Electrical Engineering, Mathematics and Computer Science. I also appreciate the support I got from him and his sincere interest in his students.

I am also grateful to all my friends and fellow students. We had a lot of fun. I would like to thank the Royal Netherlands Army. They gave me the opportunity to study and finish this MSc. program.

Finally, I would like to thank my family for their support and understanding. The study placed a heavy burden not only on me, but on my wife and children as well.

Introduction 1

Indoor ranging and positioning have got a lot of attention because of the various possible applications. In logistics businesses, the necessity of accurate tracking and tracing of stock is of high importance. Another application that requires accurate ranging and/or positioning, is for emergency/aid services. Here emergency services need to know the exact location of their personnel in a disaster area. A military application is for instance, when special units must intervene in a hostage situation in buildup areas and the commanding officer needs an overview of the area (map) and the location of its deployed personnel. Therefore, positioning and ranging of objects is nowadays an important issue.

Ranging means, measurement of the distance between a sender/receiver system and the object of interest. This is depicted in figure 1.1.

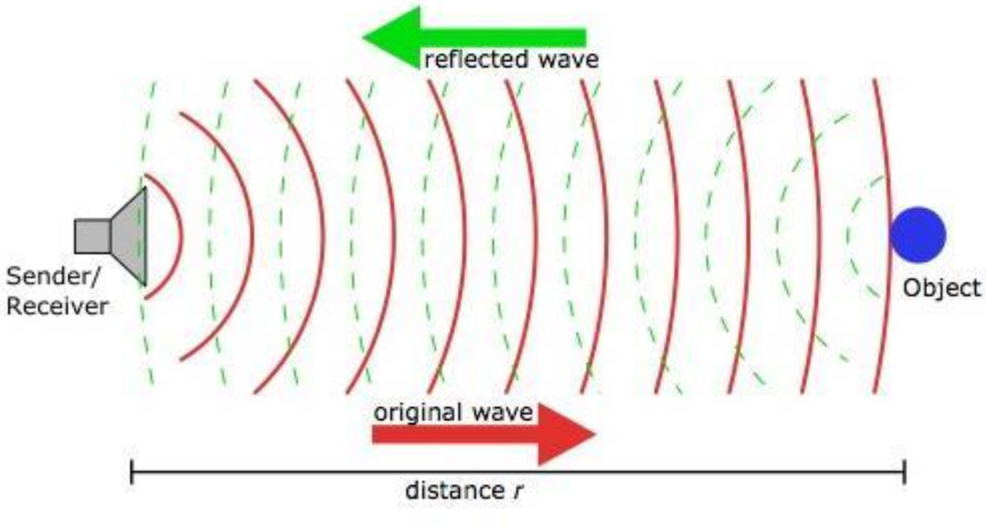

Figure 1.1 Ranging by use of radio wave [1]

With positioning is meant the computation of the location coordinates of an object of interest. This is depicted in figure 1.2. Satellite systems (like GPS) dominate the positioning market for outdoor applications, mainly due to the high accuracy and the great ease in usage. To give an impression about the accuracy, GPS can be accurate up to several meters. This depends on the used GPS configuration and signal quality. Regular GPS can be accurate up to 15 meter. DGPS can be accurate up to 3 meters [2]. Ranging systems based on Radar, are mainly developed for long distance ranging and therefore not equipped for indoor situations.

Positioning systems like GPS, are not suitable for indoor positioning, because their signals cannot penetrate buildings (too much attenuation) or the penetrated signals are too much deteriorated resulting in very inaccurate ranging information which leads to positioning errors. Therefore, alternative indoor ranging and positioning systems are needed. This thesis investigates ranging in indoor environments based on UWB FMCW signals.

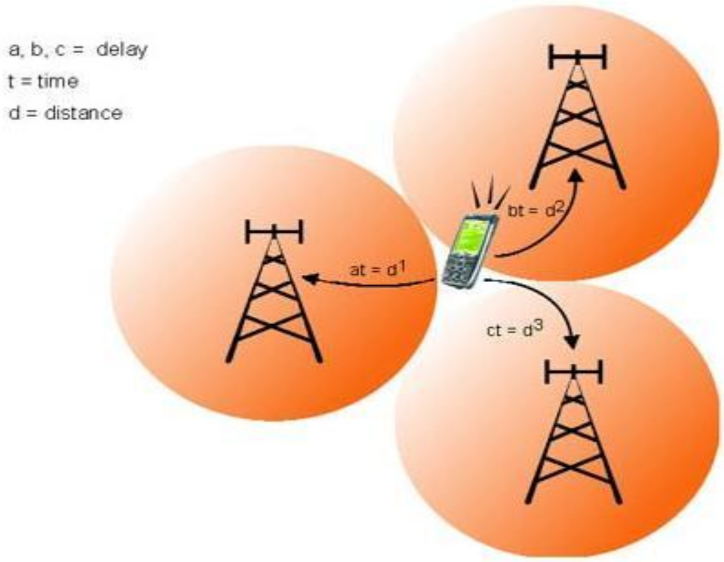

Figure 1.2 Positioning [3]

The physical structure of indoor environments causes radio waves to reflect from and diffract around obstacles. Due to these phenomena the transmitted signal most often reaches its destination (receiver) by more than one path. This is called multipath propagation. Indoor environments are called 'dense multipath environments' because of the high number of multipaths. For indoor environments UWB techniques are very promising because with this technique multipath components are resolvable. This is due to the fact that an UWB signal has a very narrow pulse width in time domain. The pulse width is smaller than the delay spread of the wireless channel, Therefore the multipaths are received in sequential order which enables the multipath components to be distinguishable.

UWB systems are systems operating with a very large bandwidth. For systems to be characterized as UWB systems, the FCC (Federal Communications Commission) proposed a definition for UWB transmission.

The definition is given by:

$$B_f = \frac{B}{f_c} = \frac{f_H - f_L}{f_H + f_L\ \ /2} \geq 0.2 \quad \text{or} \quad B \geq 500\text{MHz}, \tag{1.1}$$

where B is the signal bandwidth, B_f is the fractional bandwidth, f_c is the centre frequency and f_H and f_L are the highest and lowest transmitted frequencies at the -10dB emission point, respectively. To avoid interference with other existing radio communication systems, which may operate within the UWB bandwidth, the FCC proposed regulations concerning the power emission of UWB systems in an, for UWB systems, unlicensed frequency band of 3.1-10.6 GHz [4]. Outside this band, no intentional emissions are allowed.

For each specific frequency band, a maximum EIRP (Effective Isotropic Radiated Power) is allowed. For indoor and outdoor applications the FCC assigned two separate emission 'Masks'. In our case, only the 'Mask' for indoor applications is of interest. This Mask is depicted in figure 1.3 and in Table 1.1.

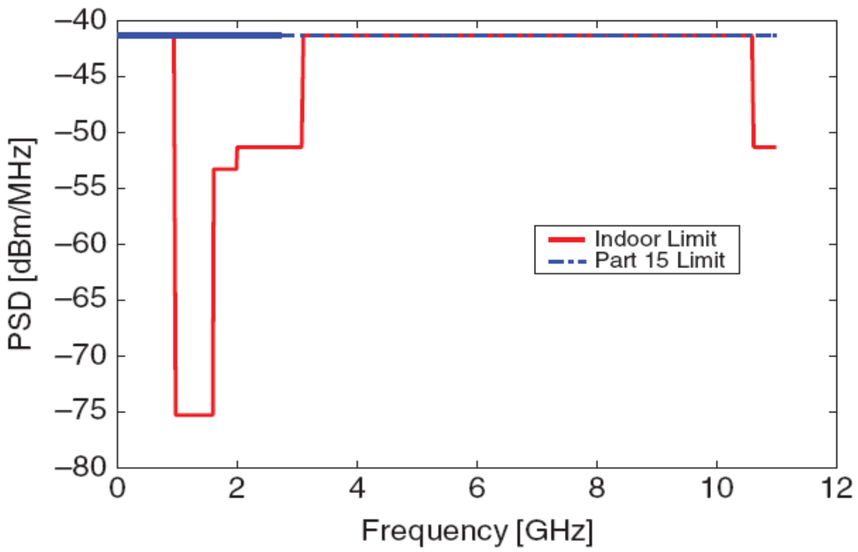

Figure 1.3. FCC Emission Limits for indoor UWB communication systems [5]

Frequency Ranges	Indoor EIRP (dBm/MHz)
960 MHz–1.61 GHz	–75.3
1.61 GHz–1.99 GHz	–53.3
1.99 GHz–3.1 GHz	–51.3
3.1 GHz–10.6 GHz	–41.3
Above 10.6 GHz	–51.3

Table 1.1. Emission Limits for indoor UWB communication systems [5]

For the peak EIRP, the FCC requires the peak emission to be limited to 0 dBm EIRP within a 50 MHz bandwidth centered around the frequency of maximum emission. The average EIRP may not exceed the level of -41.25 dBm/MHz (or 75 nW/MHz) [6] and [5].

UWB techniques offer a number of advantages compared to conventional narrow band signals. First, due to the very narrow pulses, the UWB receiver can resolve the different multipath components. This makes the UWB technique robust against multipath fading. Rake receivers can be used to retrieve the different multipath components. In this way the LOS (line of Sight) component can be distinguished and used for measuring the time delay of a received pulse (as depicted in figure 1.1). This makes UWB suitable for ranging. Second, UWB systems can coexist with narrow band communication systems. UWB has a low level of interference, because the energy is spread over a very wide frequency band. Third, UWB systems provide good obstacle penetration capabilities. Despite all the benefits, some challenges remain. These challenges are, the generation, the reception and the processing of UWB signals.

Promising indoor ranging techniques, based on the ToA principle, are pulse-based ranging and ranging by use of Frequency Modulated Continuous Wave (FMCW) signals. Reference [7] explains, by simulation and equations, how the range information is obtained. In pulse-based ranging, short duration pulses are transmitted with high peak power and low duty cycle. This is depicted in figure 1.4. The return time is a measurement for the travelled distance.

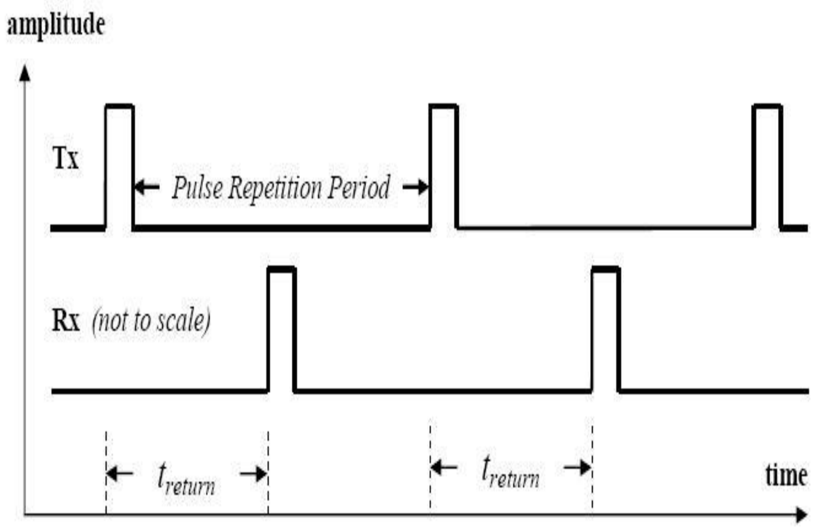

Figure 1.4 Pulse-based ranging [8]

Reference [9] elaborates more on the FMCW technique used for ranging. In this case a frequency modulated continuous wave is transmitted with a linear frequency sweep as depicted in figure 1.5.

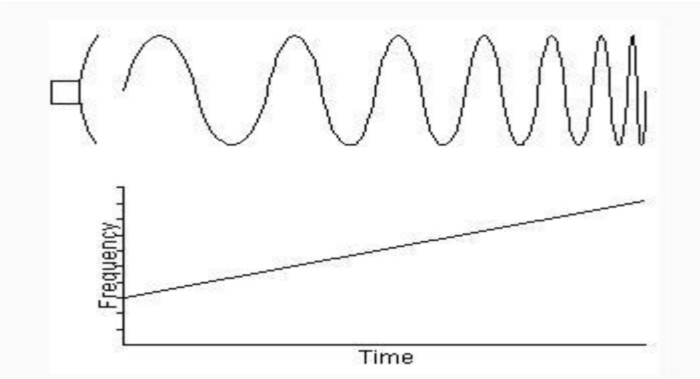

Figure 1.5 FMCW signal

Figure 1.6 depicts a transmitted FMCW signal and a (delayed) received replica. Processing the received signal reveals the beat frequency. This beat frequency is a measurement for the delay time and this delay time is proportional to the travelled distance.

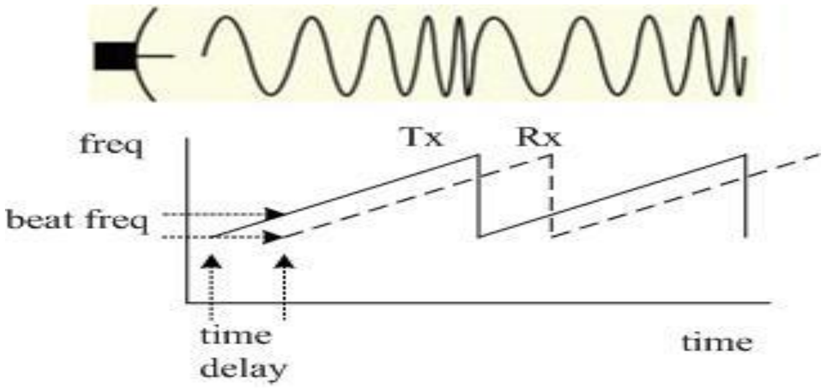

Figure 1.6 transmitted and received FMCW signal

The main advantages of FMCW are the low peak power of the transmission, the relatively large amount of energy contained by the signal (compared to pulse ranging) and the simple processing of the received signals.

This thesis contributes to a research, conducted at the Delft University of Technology, which focuses on indoor ranging based on UWB radio signals. A derived thesis subject is to investigate the performance of indoor ranging using UWB FMCW signals in the presence of noise or other (interfering) communication systems.

The focus of this thesis is on analyzing the UWB FMCW receiver system in the presence of AWGN. AWGN deteriorates the received UWB FMCW signal. For UWB FMCW ranging, it is especially important to know how AWGN deteriorates the frequency components of the receiver's output signal, because its frequency spectrum contains the time delay information and, indirectly, the range information.

The structure of the thesis is as follows. In Chapter 2 the fundamentals of the UWB indoor environment are described by explaining the propagation characteristics of the UWB indoor wireless channel. Chapter 3 describes the fundamentals of Ranging and Positioning. In Chapter 4 the fundamentals of FMCW ranging are described. In Chapter 5, the influence of AWGN on the UWB FMCW receiver system is analyzed and simulated. Finally Chapter 6 discusses the conclusions, as well as future work to be carried out.

Fundamentals of UWB Indoor Environment 2

This chapter describes the UWB propagation and explains why the UWB technique is chosen for indoor applications. It is organized as follows. First, a description of the indoor environment is given. Then, the Path Loss and Large Scale Fading are described. Next, the UWB Channel Model and Small Scale Fading are described. Finally, the key benefits of UWB are discussed and is shown why UWB is chosen for indoor ranging.

2.1 Indoor Environment and the related Radio Wave Propagation

Indoor environments are environments which are limited in dimensions due to man-made physical borders (like walls, floors and ceilings). Examples of indoor environments are, domestic rooms, industrial areas, offices, exhibition halls, railway stations, corridors and stairways. In these environments the propagation of radio waves behaves differently from outdoor environments. The physical limitations of indoor environments affect the radio wave propagation. Channeling of energy can occur, especially in corridors at high frequencies. Radio waves (partially) penetrate through walls, floors and other obstacles, giving rise to path loss and temporal and spatial variation of the signal attenuation. Due to the dense indoor multipath environment, the receiver receives the LOS path and the reflected NLOS (non Line of Sight) paths which we further refer to as multipaths. These multipaths have different arrival times and experience different attenuation and are combined at the receiver. They can add up destructively or constructively, resulting in a distorted version of the original transmitted signal. In case of resolvable multipath components, a sequence of delayed and attenuated multipath components are received for each transmitted signal. Multipath propagation can seriously degrade the performance of communications systems inside buildings. Finding a way to deal with the multipath phenomena is crucial for the performance of an indoor wireless system.

2.2 Path Loss and Large Scale Fading

The attenuation of radio waves can be split into three processes. First, attenuation due to the fact that the energy of the radio wave spreads out over an increasing area. This is referred to as path loss. Second, attenuation due to blocking of radio waves by obstacles. This is referred to as large scale fading or shadowing. Third, attenuation due to small scale fading which is due to multipath propagation.

2.2.1 Path Loss

The path loss $L(d, f)$ is a function of the distance and of the frequency, which is described by reference [5], [10] and [11]. The distance dependency of the path loss is given by:

$$L(d) = L(d_0) + 10\eta \log_{10}\left(\frac{d}{d_0}\right) \quad \text{[dB]}, \tag{2.1}$$

Where $L(d_0)$ is the free space loss at a reference distance d_0 (in the far-field region of the antenna). This is given by:

$$L(d_0) = \left(\frac{\lambda}{4\pi d_0}\right)^2, \tag{2.2}$$

d_0 is usually taken 1m for indoor environments. For $d > d_0$, the path loss is depending on the value of η, which depends on the propagation environment. Reference [12] shows that η can be obtained from measurements for different environments. Reference [10], which describes a statistical model for UWB propagation, shows example values of η. In case of LOS industrial environment η has a value of 1.63 and for NLOS industrial environment η has a value of 3.07.

For UWB systems, the path loss at different frequencies can differ noticeably. The attenuation and the effect of the propagation (reflection, etc.), changes when the frequency changes. This is due to the dispersive properties of the material of the objects which interact with the radio waves. The dispersive properties are depending on the dielectric constants of the objects material. Reference [13] discusses the ‘through-the-wall’ propagation of UWB signals and shows the effect of different object materials.

The frequency dependency of the path loss is given by eq. (2.3). Here $H(f,d)$ is the channel transfer function and Δf is chosen small enough so that the diffraction coefficients and the dielectric constants can be considered constant.

$$L(f,d) = E\left\{ \int_{f-\Delta f/2}^{f+\Delta f/2} \left| H(f',d) \right|^2 df' \right\} \tag{2.3}$$

The path loss as a function of distance and frequency can be written as a product of the distance dependency part and the frequency dependency part (as discussed in [10]). This is given by:

$$L(f,d) = L(d)L(f) \tag{2.4}$$

$L(f)$ in dB is given by:

$$L(f) = 10\kappa \log_{10}(\frac{f_0}{f}) \quad [\text{dB}], \tag{2.5}$$

where κ is a frequency dependency decaying factor. In free space κ is 1 [11]. Reference [14 shows example values of κ for different environments. f_0 is the reference frequency for which free-space is valid. The total distance and frequency depending path loss is then given by:

$$\begin{aligned} &L(f,d) = L(f_0,d_0) + L(d) + L(f) = \\ &L(f,d) = L(f_0,d_0) + 10\eta \log_{10}\left(\frac{d}{d_0}\right) + 10\kappa \log_{10}\left(\frac{f}{f_0}\right) \quad [\text{dB}], \end{aligned} \tag{2.6}$$

where $L(f_0,d_0)$ is the free-space path loss.

For an UWB signal, this frequency dependent path loss component means that signal is not only attenuated but also distorted (because the signal wave form is determined by the represented frequencies but they are attenuated differently).

2.2.2 Large Scale Fading- Shadowing

The total path loss shows random variations. These variations, also called Large Scale Fading or shadowing, are variations of the received signals strength at a fixed distance. These variations are caused by shadowing due to the presence of obstacles. According to [11], for UWB channels, the lognormal distribution can be assumed as a model for large scale fading. In the lognormal shadowing model, the ratio of the transmit-to-receive power is assumed to be random with a lognormal distribution given by:

$$p(\psi_{(\text{dB})}) = \frac{1}{\sqrt{2\pi}\sigma_{\psi(\text{dB})}} e^{-\frac{\psi_{(\text{dB})} - \mu_{\psi(\text{dB})}}{2\sigma^2_{\psi(\text{dB})}}^2}, \tag{2.7}$$

where $\psi = \frac{P_t}{P_r}$, $\mu_{\psi(\text{dB})}$ is the mean of $\psi_{(\text{dB})}$ in decibels and $\sigma_{\psi(\text{dB})}$ is the standard deviation of ψ in decibels. $\mu_{\psi(\text{dB})}$ is also referred to as the average path loss (in dB). $\psi_{(\text{dB})}$ varies with distance because the path loss increases with distance and the potential number of objects blocking the signal increases with distance. The $\sigma_{\psi(\mathrm{dB})}$ is depending on the environment. Now eq. (2.6) can be written as:

$$L(f,d) = L(f_0,d_0) + 10\eta \log_{10}\left(\frac{d}{d_0}\right) + 10\kappa \log_{10}\left(\frac{f}{f_0}\right) + \psi_{(\mathrm{dB})} \quad [\mathrm{dB}], \qquad (2.8)$$

Where $\psi_{(\mathrm{dB})}$ is a Gaussian-distributed random variable with zero mean and variance $\sigma^2_{\psi(\mathrm{dB})}$.

2.3 UWB Channel Modeling

In this paragraph, the UWB channel is characterized by means of a channel model. This paragraph describes, the UWB indoor wireless channel impulse response, the small scale fading, the distribution of the arrival times and the Power Delay Profile.

2.3.1 UWB Channel Impulse Response

For the characterization of the UWB indoor wireless channel, a time invariant situation is considered where the channel impulse response variables are (quasi) static. This time invariant wireless channel impulse response is given by:

$$h(t) = \sum_{n=0}^{N-1} a_n \delta(t-\tau_n) \qquad (2.9)$$

where N is the number of resolvable multipath components, a_n is the amplitude and τ_n is the arrival time (or time delay) of the n^{th} multipath component. $\delta(t)$ is the Dirac delta function. These variables describe the wireless channel. Wireless communication systems can be analyzed, designed and evaluated when the variables of eq. (2.9) are characterized.

2.3.2 Small Scale Fading – The Distribution of Amplitude Fading

Small scale fading is fading due to multipath effects. For UWB signals, the multipath components are resolvable. There is always a probability that several multipath components have approximately the same path length. These multipath components are received (partially) overlapping and summed. Destructive adding of these multipath components causes fading. The number of overlapping multipath components is less than when compared to conventional narrowband systems. According to A.F. Molisch [10], which describes a comprehensive statistical model for UWB propagation channel for several indoor environments valid in the frequency range of 3.1-10.6GHz, the Nakagami distribution is a good indoor model for small scale fading. The Nakagami distribution is explained as follows and depicted by figure 2.1.

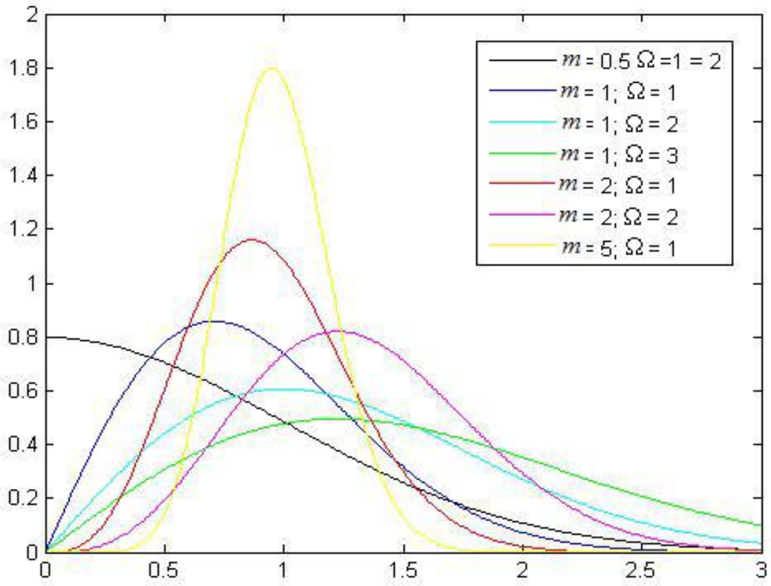

Figure 2.1 Nakagami distribution [15]

In the Nakagami distribution, the amplitude of the multipath components are random. The pdf of the Nakagami distribution is given by:

$$f(d) = \frac{2m^m d^{2m-1}}{\Gamma(m)\,\Omega^m} e^{-\frac{md^2}{\Omega}}, \qquad d \geq 0, \tag{2.10}$$

where $\Omega = E[d^2]$, $m = [E[d^2]^2 / Var[d^2]]$, and the constraint that $m \geq 0.5$. $\Gamma(m)$ is the Gamma function defined as:

$$\Gamma(m) = \int_0^\infty t^{m-1} e^{-t} dt, \qquad m \geq 0.5 \tag{2.11}$$

The Nakagami distribution is also known as the m-distribution. For $m = 1$ the Nakagami distribution behaves like a Rayleigh distribution.

The number of objects a radio wave encounters and the dielectric constants of these objects material influences the propagated radio wave. A suitable statistical model must be chosen describing the amplitude fading best. In case of the absence of a dominating multipath component, the amplitude fading is best described by a Rayleigh distribution. In the presence of a dominating multipath component, the amplitude fading is best described by a Rician distribution.

2.3.3 The Distribution of Time of Arrival

Different distribution models for the arrival times of the multipath components in wireless channels have been investigated. For UWB systems in indoor environments, the double Poisson model (or Saleh-Valenzula) is a good model [10]. In this model, arrivals occur in clusters. Figure 2.2 depicts several power delay profiles with exponentially decaying clusters and rays. The arrival times of the multipath components are distributed according to a double Poisson model.

The arrival rate of the clusters is α. Within each cluster, multipath components arrive according to a Poisson distribution with rate β. When the arrival of the rays is according to the Poisson distribution, the inter-arrival times are exponentially distributed. If T_l is the arrival time of the l^{th} cluster, the probability of T_l given T_{l-1} is:

$$\text{Prob}(T_l \,|\, T_{l-1}) = \alpha e^{-\alpha (T_l - T_{l-1})} \tag{2.12}$$

For the arrival time of the n^{th} arrival in the l^{th} cluster, the probability is given by:

$$\text{Prob}(\tau_{n,l} \,|\, \tau_{n-1,l}) = \beta e^{-\beta (\tau_{n,l} - \tau_{n-1,l})} \tag{2.13}$$

The impulse response of the UWB wireless channel becomes:

$$h(t) = \sum_{l=0}^{\infty} \sum_{n=0}^{\infty} a_{n,l} \delta(t - T_l - \tau_{n,l}) e^{j\theta_{n,l}} \tag{2.14}$$

2.3.4 Power Delay Profile and the RMS Delay Spread

The Power Delay Profile (PDP) represents the average power associated with a given multipath delay [12], [16]. By using the impulse response of the channel, the received power can be obtained as:

$$P(\tau_n) = E\left[\left|h(t)^2\right|\right] = \sum_{n=0}^{N-1} \overline{a_n^2} \delta(t - \tau_n) \tag{2.15}$$

The multipath components which experience a longer delay are usually more attenuated.

The power delay profile of clustered UWB channels can be expressed by two non-negative exponential function. This is given by:

$$P_{n,l} = P_{0,0} e^{-T_l / \Gamma} e^{-\tau_{n,l} / \gamma} \tag{2.16}$$

Where $P_{0,0}$ is the received power of the first path of the first cluster. And γ and Γ are the multipath and cluster time decay constants of the power delay profile, respectively. The power delay profile of an UWB channel is depicted in figure 2.2.

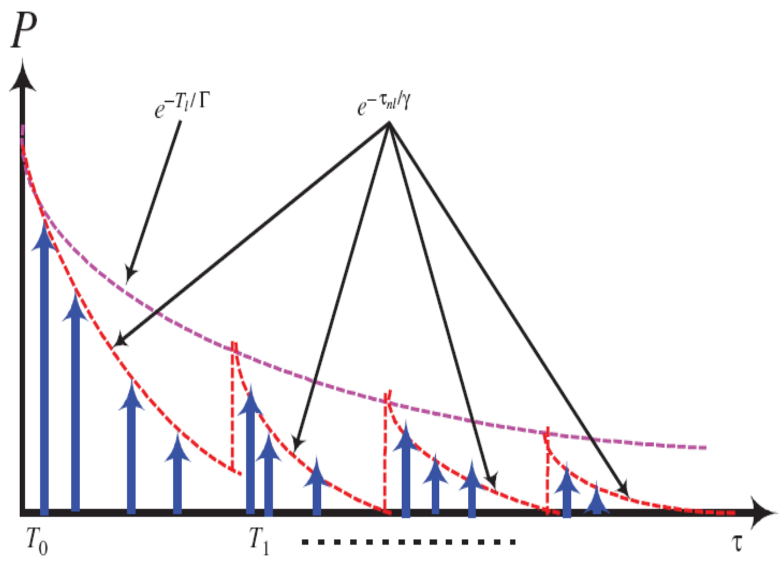

Figure 2.2 Several power delay profiles with exponential decaying cluster and rays; resource [5]

The RMS Delay Spread

Where the PDP shows the average received power related to the multipath delay, the RMS (Root Mean Square) delay spread is the standard deviation of the delay of the multipath components. It indicates the degree of multipath spread of the channel. From the PDP, the RMS delay spread (τ_{rms}) can be easily calculated.

The calculation of τ_{rms} is given by:

$$\tau_{rms} = \sqrt{\overline{\tau^2} - \bar{\tau}^2} \tag{2.17}$$

Where $\bar{\tau}$ is the mean excess delay (or the first moment of the power profile) and $\overline{\tau^2}$ is the second moment of the power profile, given by eq. (2.18) and eq. (2.19) respectively:

$$\bar{\tau} = \frac{\sum_i a_i^2 \tau_i}{\sum_i a_i^2} = \frac{\sum_i P(\tau_i)\tau_i}{\sum_i P(\tau_i)} \tag{2.18}$$

$$\overline{\tau^2} = \frac{\sum_i P(\tau_i)\tau_i^2}{\sum_i P(\tau_i)} \tag{2.19}$$

The performance of the radio communication system operating in the wireless channels is very sensitive to the value of τ_{rms} .

For a signal with symbol period T_s, the system experiences ISI (Inter Symbol Interference) if $T_s < \tau_{rms}$. This significantly degrades the performance of the communication system. In case where $T_s >> \tau_{rms}$, the system experiences negligible ISI.

2.4 Summary

The indoor environment is characterized by limited dimensions and multiple obstacles. The objects cause radio waves to reflect, diffract etc., resulting in multipath propagation. This causes an indoor environment to be a dense multipath environment.

UWB radio waves experience attenuation which is referred to as propagation loss. Propagation loss can be split up in three part namely, path loss, large scale fading and small scale fading. Due to the dispersive properties of obstacles, a frequency dependent loss component is added. These dispersive properties are depending on the dielectric constants and the diffraction coefficients of the obstacles material.

The UWB Channel Impulse Response is characterized by two random variables, respectively the amplitudes and the arrival times of the multipath components. The amplitude distribution model for UWB indoor communication systems is best described by the Nakagami distribution and the arrival time distribution is best described by the double Poisson distribution.

The RMS Delay Spread is a good measure of multipath spread of the wireless channel and the Power Delay Profile expresses the power associated to the delayed multipath components.

The benefits of UWB in indoor environments are; the ability to coexists with narrow band communication systems due to the FCC power regulations, the resolvability of the multipath components (which makes UWB systems multipath robust) and the good material penetrating capabilities (which allows UWB systems to operate in environments with many obstacles). These features cause the UWB technique to be favorite for indoor applications. Note, that UWB signals that penetrate obstacles experience attenuation and distortion due to the dispersive properties of obstacles.

Principles of Ranging and Positioning Techniques 3

Ranging and positioning systems require a certain system design. It can be designed (for instance) for navigation application or for tracking/monitoring applications with medium or high accuracy. Depending on the application a ranging and positioning system is designed according to a certain network topology. For the accuracy requirement, different methods can be used to obtain medium or high accurate ranging and/or positioning information. This chapter describes the two types of network topologies and three different methods for obtaining ranging and/or positioning information.

3.1 Network Topologies

Most existing positioning systems are build up according to one of two popular network topologies, which are described by [6]. These topologies are called the Network Based System (used for tracking/monitoring applications) and the Handset Based System (used for (self)navigation applications). Figure 3.1 and figure 3.2 depict the Network Based System and the Handset Based System respectively.

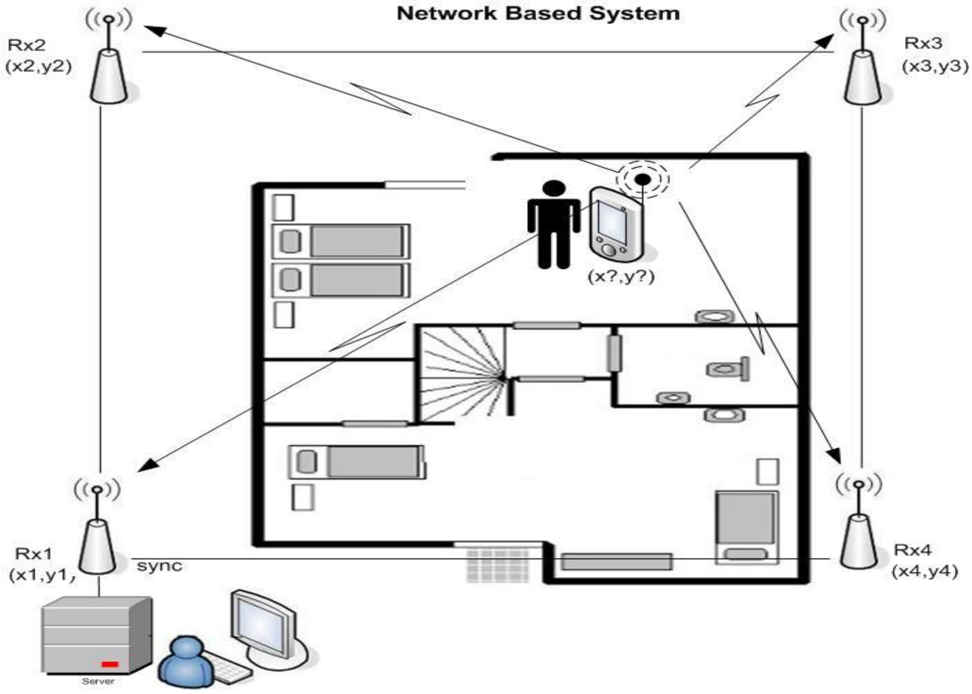

Figure 3.1 Network Based System

In the Network Based System, several receiver stations (with known positions) receive the signal send by a small transmitter (mobile device) which is carried by an individual or an object. Each station receives this signal with some time delay. The time delayed signals are send to a control station. From the time delay information, a control station computes the actual location of the object. The location information is only known at the control station.

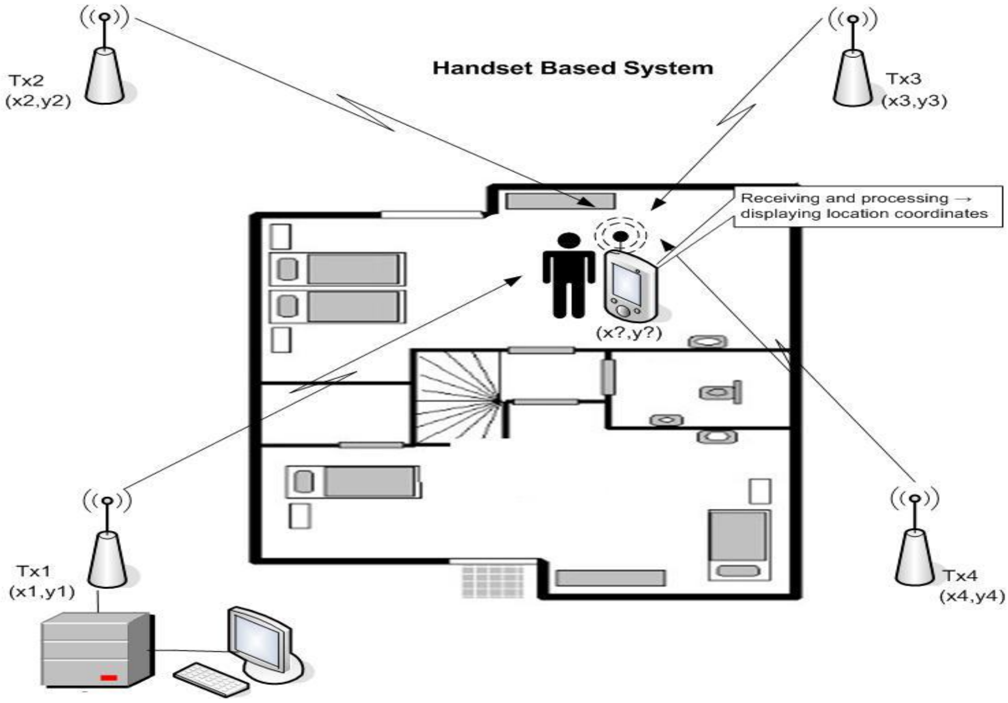

Figure 3.2 Handset based System

In the Handset Based System, all (fixed positioned) reference stations transmit a (unique) signal. The mobile device knows the locations of these transmitters and knows their signal format. These transmitted signals are received by the mobile device with some time delay. From the time delay information, the handset computes its own location. The mobile device conducts the actual data processing and data logging. This demands integration of technology of higher complexity.

The main advantage of the Network Based System is, that its mobile device (which only sends a signal) has low hardware complexity. In many cases a RF beacon suffices.

The main advantage of the Handset Based System is the freedom of movement of the user and the privacy of user location information.

3.2 Methods to obtain Ranging and/or Positioning Information

Different methods can be used to obtain ranging and/or positioning information. These methods are (for instance) based on the angle of arrival (AOA) principle, the received signal strength (RSS) principle or the time of arrival (T(D)OA) principle. These principles, described by [5] and [6], are the most commonly known methods.

3.2.1 Received Signal Strength (RSS)

The RSS ranging method is used in Network Based Systems as well as in Handset Based Systems. Technically, the signal strength of the received signal is compared with the signal strength of the original transmitted signal. The distance travelled by the signal can be estimated from Friis Transmission Equation. This principle is suitable when the received signal travels the direct path between transmitter and receiver. If the received signal is not the direct path signal, it has a longer path length and is therefore more attenuated. Ranging based on indirect path signals causes large range errors. Figure 3.3 depicts RSS based ranging with a Network Based System topology. In case of 2D positioning, a minimum of three reference nodes are required. At each reference node, a range circle is computed and in ideal circumstances these range circles will intersect in location (x_0, y_0). Thus, the location of the handset can be found by solving x_0 and y_0 from the distance equations given by:

$$d_i = \sqrt{(x_i - x_0)^2 + (y_i - y_0)^2} \tag{3.1}$$

The index i indicates the reference node number and d_i is the distance from that reference node to the mobile device. Exact knowledge of the path loss and the path loss exponent (of that environment) is necessary for accurate ranging. In practice, different range circles will not intersect in one spot because of multipath effects and measurement flaws.

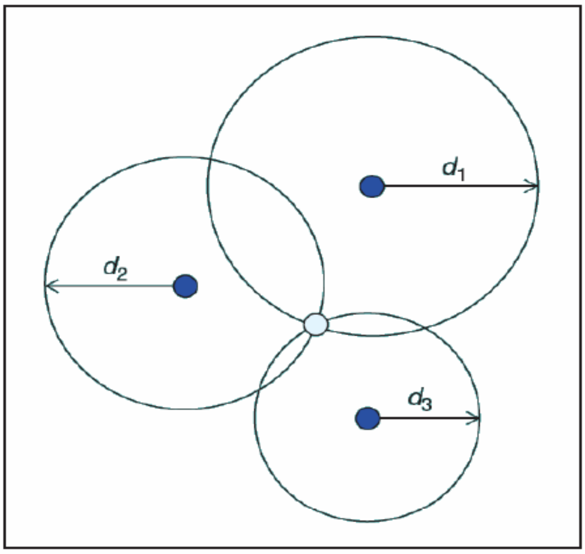

Figure 3.3 Received Signal Strength (RSS) positioning technique

Applying RSS to the Handset Based System, the mobile device must be able to distinguish each received signal and know its exact location of transmission. This can be done by, for example, signal signature coding for each transmitter. The high sensitivity to multipath propagation is a disadvantage of the RSS technique because it causes range errors.

3.2.2 Angle of Arrival (AoA)

The AoA method measures the angle of an incoming signal by two or more directional sensitive receiving antennas. This technique is mainly used in Network Based Systems, because the necessary directional antennas or antenna array's are related to a specific orientation and a geographical location. In addition, the integration of such antenna array in a mobile device is almost impossible.

The signal transmitted by the mobile device is received by several fixed stations. The receiver antennas (or antenna arrays) are, for instance, ideally horizontally calibrated. Meaning that their maximum reception capability is directed towards zero azimuth. For receiving maximum power, these receiver antennas turn (or redirect) their antenna beam into the direction of the transmitted signal. The angle to which the antenna (or antenna beam) is turned, is a measurement for the location of the transmitter. In ideal circumstances, the control station determines the location of the mobile device geometrically by determining the coordinates at which the radial lines intersect. In a 2D positioning environment, a minimum of two reference points is necessary. Figure 3.4 depicts the AoA principle in a two reference node model.

x_1, y_1 and x_2, y_2 are the locations of reference node 1 and 2 respectively. x_0, y_0 is the location to be determined. Angle θ_1, θ_2 are defined as:

$$\tan\ \theta_1 = \frac{y_0}{x_0}\ ,\ \tan\ \theta_2 = \frac{y_2 - y_0}{x_0} \tag{3.2}$$

The x-position of node 0 can be determined as:

$$x_0 = \frac{y_2}{\tan\ \theta_1 + \tan\ \theta_2} \tag{3.3}$$

The y-position of node 0 can be found by substituting the x-position in one of the angle definitions.

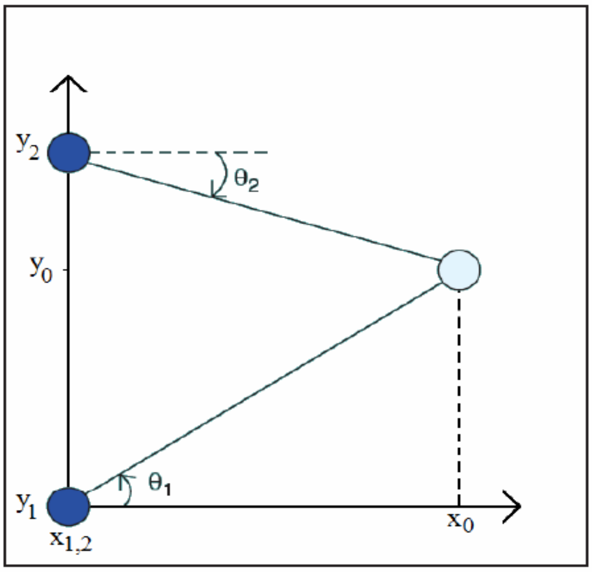

Figure 3.4 Angle of Arrival positioning technique

The principle of this positioning technique is based on the reception of a LOS signal. In practice, multipath effects and measurement flaws cause the radial lines of the used reference nodes not to intersect at the same location. This technique is very sensitive to multipath effects. An advantage is the lack of necessity of precise time references or time synchronization.

3.2.3 Time of Arrival (ToA)

The Time of Arrival principle used for ranging and/or positioning is based on the time needed for a signal to travel from the transmitter to the receiver. This method is applied in Network Based Systems as well as in Handset Based Systems. Figure 3.5 depicts the Network

Based System variant. In a 2D environment, at least three reference nodes must be available for proper positioning.

The node that has to be localized is transmitting, at a specific moment in time, a signal which is received by the reference nodes. The mobile device requires synchronization. For each of the reference nodes, the propagation delay time is computed and send to the control station. The control station computes for each reference node the corresponding traversed distance, according to:

$$d_i = c\tau_i, \tag{3.4}$$

where c is the speed of light, τ_i is the measured propagation delay time at a specific reference node i. Once the calculated distances from the transmitter to the different reference nodes are known, a range circle can be placed around the corresponding reference node (like in figure 3.3). The location of the mobile unit can now be determined by solving x_0 and y_0 from the distance equations (3.1).

The accuracy of the system depends on the quality of the time synchronization technique. A deviation of about 1ns causes a difference in distance of 0.3 meter. Time synchronization (where only the reference nodes need to be synchronized) makes the system much more complex.

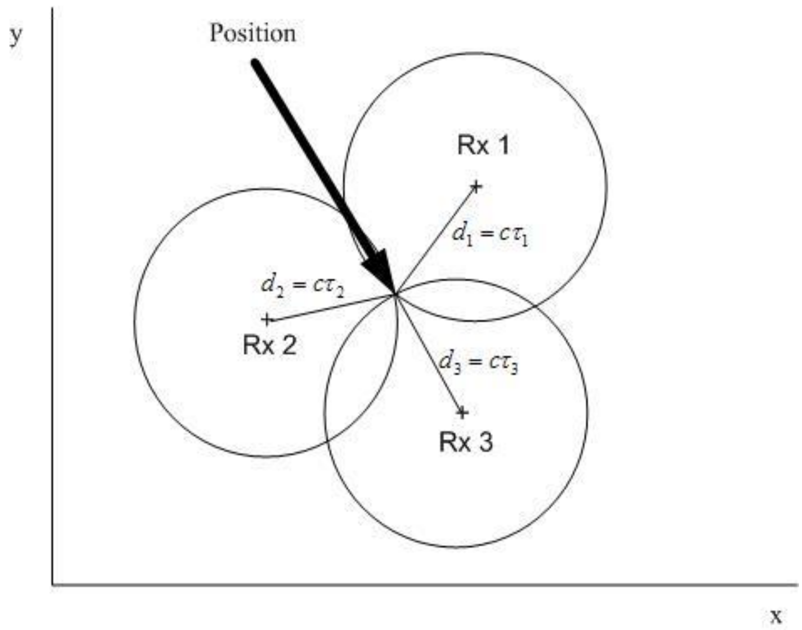

Figure 3.5 Time of Arrival positioning technique

TDoA (Time Difference of Arrival) is a variant of ToA where knowledge of the exact transmission time is no longer required, here only the reference nodes need to be synchronized. This is done by synchronization of the receiver clocks.

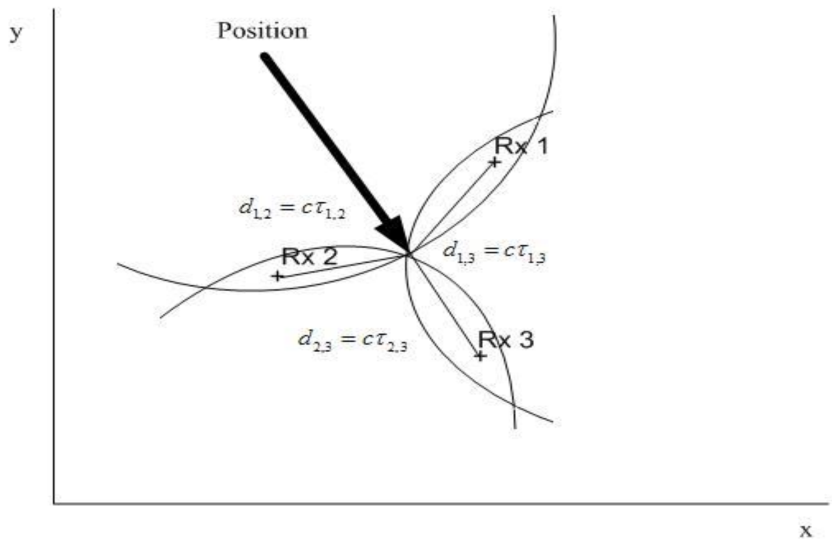

Figure 3.6 Time Difference of Arrival positioning technique

In TDoA, the differences in time, at which the signal from the mobile device arrives at the receivers, are measured. With these time differences information, hyperboloids are placed around the two relevant receivers with a constant distance difference between the two receivers. This is depicted in figure 3.6. With the next equation the distances of the hyperboloids with respect to two receivers is given.

$$d_{i,j} = c\tau_{i,j}, \tag{3.5}$$

Where $\tau_{i,j}$ is the time delay difference and the indices i and j indicate the relevant receivers. The location of the mobile unit can now be determined by solving x_0 and y_0 from the distance equations (3.5). Eventually, this type of time delay based system has an accuracy of about several centimeters, but this will increase in a dense multipath environment. For T(D)oA ranging with UWB signals, these techniques offer very accurate range and positioning information (in the order of centimeters [6]). The multipath robustness of UWB signals positively influences the accuracy.

3.3 Summary

This chapter describes the two types of network topologies and three different methods for obtaining ranging and/or positioning information.

Both the Network Based System and the Handset Based System topologies can be used for UWB indoor ranging applications. For Network Based Systems, the mobile device can be a simple device only transmitting a beacon signal. The range and positioning computations are done at the control station. For Handset Based Systems, the mobile device is more complex. It performs the data measurements and position calculation. The advantage is the privacy of the position information.

Three methods to obtain ranging and/or positioning information are discussed. For indoor applications using UWB signal, RSS and AoA perform less than T(D)oA. The disadvantage of UWB RSS is that the exact propagation loss model is needed for accurate ranging and positioning. The disadvantage of UWB AoA is that the directional antennas are large and need frequent calibration. In case of Handset Based Systems, it is very complex to apply directional antennas into a small mobile device. The advantage of UWB T(D)oA is the high accuracy and good performance in indoor environments.

Principle of FMCW Ranging

4

As the name suggests, in Frequency Modulated Continuous Wave (FMCW) ranging a continuous wave signal is used for obtaining range information. This chapter discusses the principle of ranging using FMCW signals.

4.1 FMCW signal

An FMCW ranging system transmits a signal which contains a linear frequency sweep. The signal is reflected from distant objects and detected by the receiver where the returned signal is mixed with a replica of the transmitted signal to determine the range of the object. Figure 4.1 depicts an FMCW signal with a linear frequency sweep. Here, the transmitted signal has a constant envelope and a frequency which increases linearly with time. This linear variation of frequency with time is often called a chirp. Figure 4.2 depicts the FMCW signal as frequency versus time. The frequency sweep starts with the lowest frequency f_l and stops at the highest frequency f_h. The difference between f_l and f_h is the signal bandwidth B. The duration of the sweep is T seconds.

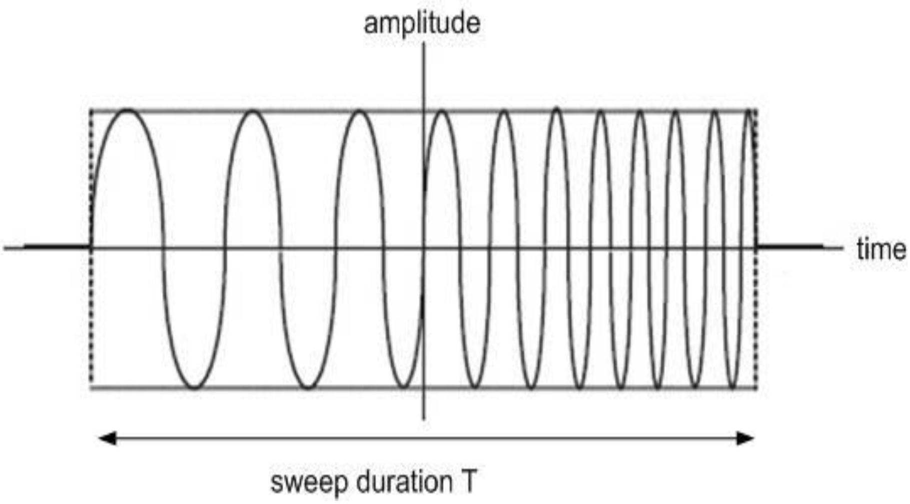

Figure 4.1 FMCW signal

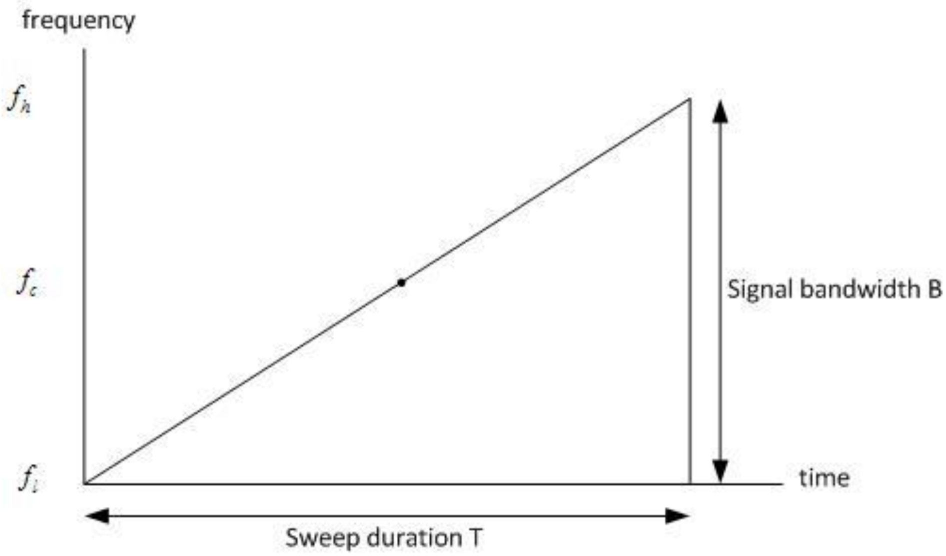

Figure 4.2 FMCW signal frequency versus time

The frequency of the transmitted signal is represented by:

$$f(t) = f_l + \zeta t \qquad \forall \ t < T, \tag{4.1}$$

Where ζ is the rate of change of frequency [Hz/s]. ζ is given by:

$$\zeta \triangleq \frac{f_h - f_l}{T} = \frac{B}{T} \ \text{[Hz/s]} \tag{4.2}$$

The phase of the signal is given by:

$$\phi(t) = 2\pi \int f(t)dt = 2\pi(f_l t + \tfrac{1}{2}\zeta t^2 + \phi_0) \tag{4.3}$$

Where ϕ_0 is the initial phase at time $t = 0$ and for simplicity $\phi_0 = 0$ is chosen.

The transmitted signal can now be given by:

$$s(t) = A_t \cos 2\pi(f_l t + \tfrac{1}{2}\zeta t^2) \ , \ 0 \le t \le T, \tag{4.4}$$

where A_t is the transmitted signal amplitude.

During the transmission of $s(t)$, a signal $r(t)$ is received. This is depicted in figure 4.3. $r(t)$ is a replica of the transmitted waveform but delayed in time with a certain delay τ_d. In case of one-way propagation, the time delay is given by:

$$\tau_d = \frac{R}{c}, \tag{4.5}$$

where c is the speed of light in the medium and R is the distance between transmitter and receiver. $r(t)$ is given by:

$$r(t) = A_r \cos 2\pi(f_l(t - \tau_d) + \tfrac{1}{2}\zeta(t - \tau_d)^2), \tag{4.6}$$

where A_r is the received signal amplitude. The maximum delay time $\tau_{d_{MAX}}$ is dictated by the environment. T is chosen in such way that $T >> \tau_{d_{MAX}}$. In this way a received signal that is processed leads to unambiguous range information.

4.2 Retrieving the Beat Frequency

In the FMCW ranging receiver (based on ToA), the received signal is mixed with a replica of the transmitted waveform and low pass filtered. The resulting output is called the beat signal. Figure 4.3 depicts the transmitted and received signal and the resulting beat signal (frequency versus time) after mixing and low pass filtering. The Fourier transform is performed on the beat signal, making the signal content available in the frequency domain, revealing the beat frequency. This beat frequency is a measure for the range as is shown in the following.

At the receiver $s(t)$ and $r(t)$ are mixed which is given by:

$$s(t)r(t) = A_t \cos 2\pi(f_l t + \tfrac{1}{2}\zeta t^2) A_r \cos 2\pi(f_l (t - \tau_d) + \tfrac{1}{2}\zeta (t - \tau_d)^2) \tag{4.7}$$

For a multiplication of two cosine functions, the next cosine rule is used:

$$\cos\alpha \cos\beta = \tfrac{1}{2}\ \cos\ \alpha + \beta\ + \cos\ \alpha - \beta \tag{4.8}$$

Applying eq. (4.8) to eq. (4.7) results in, a sum-term which is given by:

$$\frac{A_t A_t}{2} \cos 2\pi (2 f_l t + \zeta t^2 + \zeta t \tau_d - f_l \tau_d + \tfrac{1}{2}\zeta {\tau_d}^2) \tag{4.9}$$

and a difference-term which is given by:

$$\frac{A_t A_t}{2} \cos 2\pi (\zeta \tau_d t + f_l \tau_d + \tfrac{1}{2}\zeta {\tau_d}^2) \tag{4.10}$$

In the FMCW ranging system receiver, a Low Pass Filter (LPF) is applied to $s(t)r(t)$ in such way that only the difference term eq. (4.10) is allowed to pass. This LPF output signal is called the beat signal $b_s(t)$ and is given by:

$$b_s(t) = \frac{A_t A_r}{2} \cos 2\pi (f_l \tau_d + \zeta t \tau_d + \tfrac{1}{2}\zeta \tau_d^2), \quad \tau_d \le t \le T \tag{4.11}$$

The beat frequency can be derived from eq. (4.11) by taking the derivative of the phase [17]. This is given by:

$$f_b = \frac{1}{2\pi} \frac{d(\phi_{bs(t)})}{dt} \tag{4.12}$$

The resulting beat frequency is then:

$$f_b = \zeta \tau_d \tag{4.13}$$

From figure 4.3, it can be seen that the frequency of the beat signal is directly proportional to the time delay, and hence to the distance. This holds only for $\tau_d \leq t \leq T$. For $T \leq t \leq T + \tau_d$ the beat frequency provides false range information. Choosing ζ steep enough so that the beat frequency component related to $\tau_d \leq t \leq T$ is smaller than the beat frequency component related to $T \leq t \leq T + \tau_d$. The latter part can be excluded by filtering. Substituting eq. (4.5) in eq. (4.13) gives:

$$f_b = \frac{\zeta R}{c} = \frac{BR}{cT} \tag{4.14}$$

and the distance is given by:

$$R = \frac{c f_b T}{B} \tag{4.15}$$

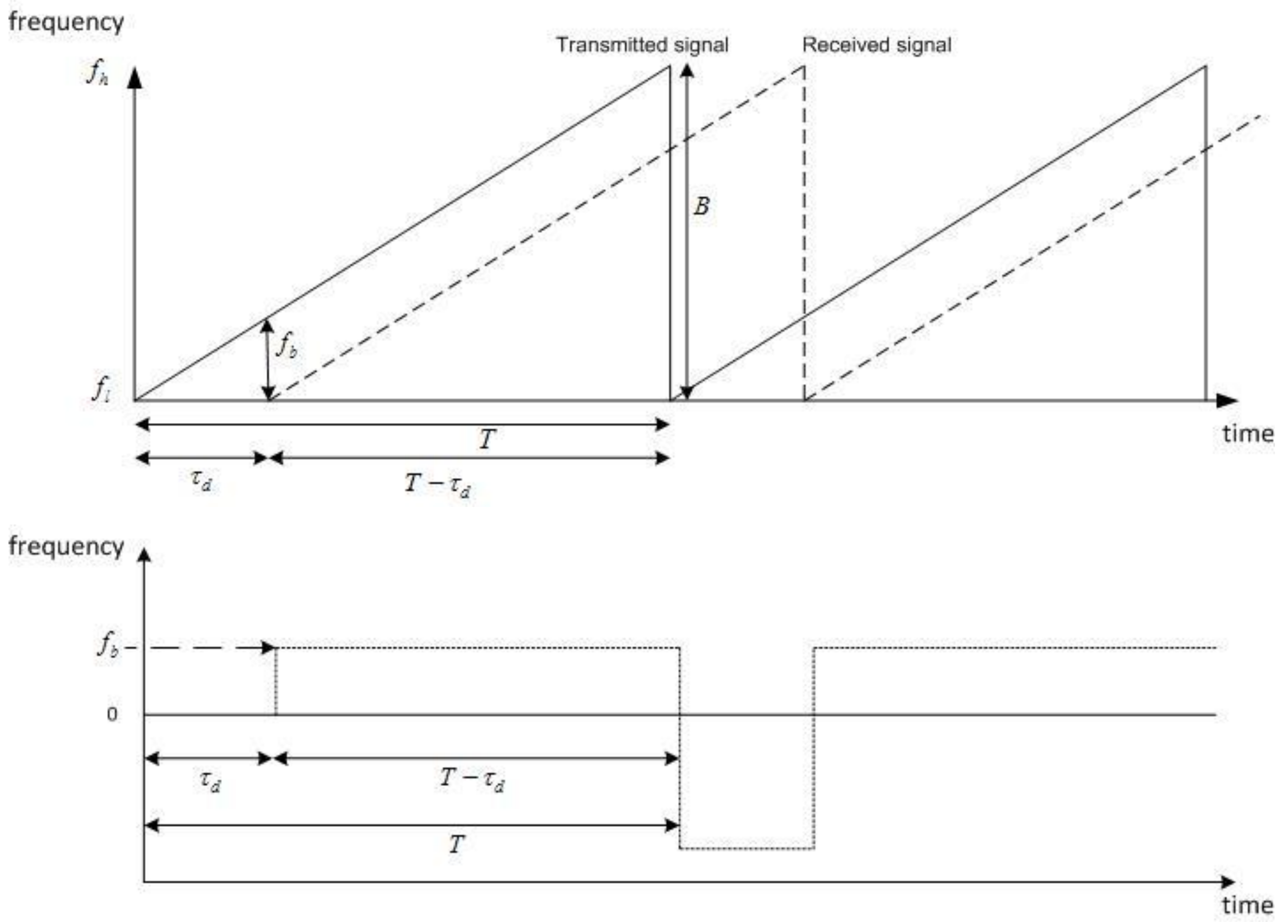

Figure 4.3 The beat frequency

Non linearity of the frequency sweep causes the beat frequency to vary. This results in range errors.

For multipath propagation $r(t)$ is given by:

$$r(t) = \sum_{n=1}^{N} a_n s(t - \tau_n) \tag{4.16}$$

Substituting $s(t)$ of eq. (4.4) into eq. (4.16) and applying the LPF results in:

$$b_s(t) \overset{LPF}{=} \sum_{n=1}^{N} \frac{a_n}{2} \cos 2\pi(f_l \tau_{d_n} + \zeta t \tau_{d_n} + \tfrac{1}{2} \zeta \tau_{d_n}^2), \quad \tau_{d_n} \le t \le T \tag{4.17}$$

In figure 4.4, the transmitted and received multipath components are depicted. Each delayed multipath components represents a different beat frequency (with a frequency not exceeding the cut-off frequency of the LPF). The larger the used signal bandwidth, the more the different beat frequencies (corresponding to the different delayed multipath components) are spaced in frequency and therefore distinguishable. This enables the FMCW ranging system to select the beat frequency corresponding to the direct path and provide proper range information.

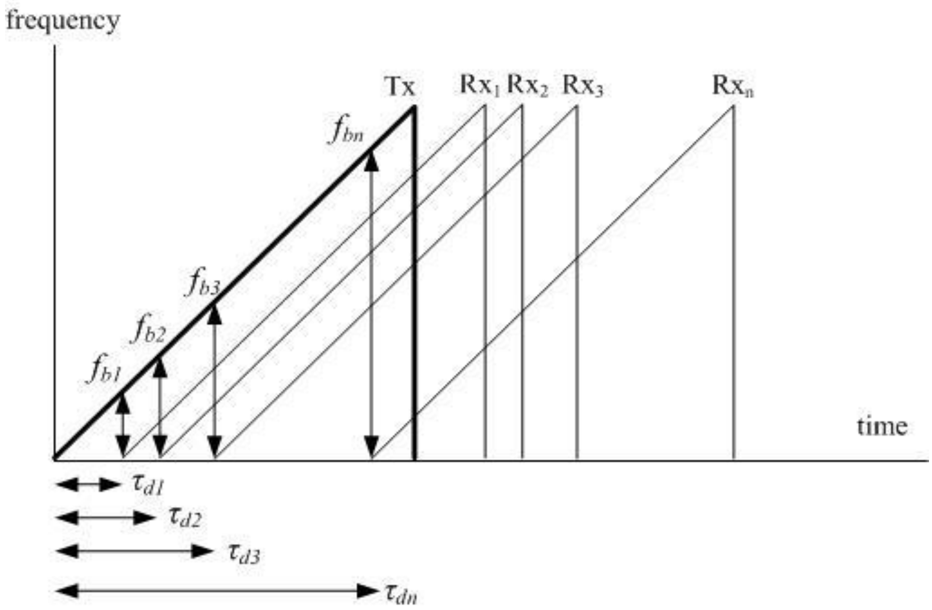

Figure 4.4 FMCW multipath components

4.3 FMCW Ranging versus Pulse Ranging

This paragraph discusses some features of FMCW ranging and Pulse ranging. These features are described in reference [8].

Both ranging techniques are based on ToA and use the time delay of the received signal as a measure for its travelled distance. The important difference is how they obtain the (estimated) delay time. Where pulse ranging transmits a pulse and measures the time it takes to return, FMCW transmits a continuous signal (which varies in frequency) and compares the instantaneous frequencies of transmitted and received signal. This frequency difference is a measure for the time delay and hence proportional to the distance.

In a pulse-based ranging system the pulse width is inversely proportional to the bandwidth. For indoor ranging (small RMS delay spread) only narrow pulses cause multipaths to be resolvable, which leads to proper range information. The main disadvantage is to generate very narrow high power pulses and to process these pulses. In case of FMCW ranging, pulses (frequency sweeps) have a relatively long duration, and therefore, can contain more energy. High energy (received) signals lead to higher SNR, which positively affects the processed range information.

For both ranging systems the maximum range is limited by the pulse repetition period. In order to generate unambiguous range information the pulse repetition period should be larger than the maximum time delay of received pulses.

For mono-static ranging systems, the pulse based system is blind for reception at the moment of transmitting a pulse. For FMCW ranging, transmission and receiving is done simultaneously. A challenge for FMCW is to avoid direct leakage from transmitted pulse into the receiving antenna.

For indoor ranging with UWB signals, the indoor environment determines the corresponding RMS delay spread (this is in the order of 100ns [14]) and the FCC determines the maximum transmit power per frequency range. An echo (or received pulse) is detected properly if it contains enough energy. The larger the amount of contained energy, the better the detection performance. UWB FMCW ranging performs better on this aspect than UWB pulse ranging due to the large duty cycle (100%) and its maximum average transmit power (FCC). Therefore an UWB FMCW echo contains more energy than an UWB pulse echo. Although an UWB pulse has a higher peak power, the average energy is lower due to the small pulse width and the small duty cycle.

FMCW is chosen for UWB indoor ranging because of its simpler signal processing, because it can measure very short distances and because its signal contains more energy. This results in good detection performance.

4.4 Summary

This chapter describes the principle of FMCW ranging. In stead of ranging by transmitting narrow pulses (like pulse based ranging), FMCW transmits a frequency modulated continuous wave. This FMCW signal is reflected from distant objects and detected by the receiver where the returned signal is mixed with a replica of the transmitted signal. The result is LPF filtered, selecting only the beat frequency which is proportional to the range of an object. This only holds for a the period $\tau_d \leq t \leq T$.

The maximum range of the FMCW ranging system is related to the time duration of the FMCW sweep. A received signal with a time delay larger than the sweep duration causes ambiguous range information, thus $\tau_{d_{MAX}} << T_{sweep}$. In case of multipath propagation, all received multipaths (with time delays smaller than the sweep duration) introduce different beat frequencies. Providing a FMCW signal with a large bandwidth and a large sweep duration, enables the different beat frequencies (corresponding to the different multipath components) to be spaced in frequency. This makes it easier to distinguish them and therefore enables the FMCW receiver to select the direct path component and derive the corresponding range information.
Than comparing UWB pulse ranging and FMCW ranging, FMCW echo's contain more energy than a pulse echo. High energy (received) signals leads to better SNR which positively affects the processed range information. A main drawback is that the frequency sweep must be pure. Non linearity of the frequency sweep causes deviation in the beat frequency resulting in range errors.

FMCW is mainly chosen for UWB indoor ranging because: its simple signal processing, it can measure very short distances, its signal contains more energy resulting in better detection.

Noise Analysis and Simulation 5

This chapter discusses the UWB FMCW receiver process and the analysis and simulation of the influence of Additive White Gaussian Noise (AWGN) on ranging (AWGN is further addressed as 'noise'). The organization of this chapter is as follows. Paragraph 5.1 presents the problem description and the approach to investigate the problem. In paragraph 5.2, a block diagram is given of the UWB FMCW receiver, explaining the receiver process and introducing the system variables in a mathematical framework. Next, paragraph 5.3 describes the analysis of the receiver process. In paragraph 5.4, UWB FMCW system parameters are given and simulations are conducted to verify and/or validate the analysis. Finally, a summary is given in paragraph 5.5

5.1 Problem Description and Investigation Approach

Problem description

What is the effect of noise on ranging using UWB FMCW signals and how does noise influence the UWB FMCW ranging system's maximum range and what kind of range estimation errors do occur.

Noise deteriorates a signal by affecting its amplitude and phase. In pulse based ranging systems, where the received ranging signal is evaluated in the time domain, a received pulse can only be properly detected if its amplitude exceed a certain threshold. Below this threshold the amplitude of the signal is assumed to be too much distorted by the noise for proper detection.

Evaluating a signal in the frequency domain, the noise distortion of the signal's phase causes its frequency spectrum components to be deteriorated. For FMCW ranging, range information is derived from the frequency spectrum of the beat signal. Thus, deterioration of the signal's frequency components corrupts the multipath delay information, and therefore, the range information.

In this thesis, the effect of noise on UWB FMCW ranging is analyzed. Meaning that the analysis is focused on the impact of noise on the UWB FMCW beat signal frequency components.

Investigation approach

Noise is a random process, therefore it cannot be described deterministically. A good way to describe a random process is by its statistical properties (mean, standard deviation, distribution and whether it's a stationary process or not). From these statistical properties, we can derive the average power and power spectral density of the random process. The calculation of the autocorrelation function of the random process is a good tool for this, because there is a direct relation between the autocorrelation and the power spectral density.

The UWB FMCW receiver is analyzed step by step by calculating the auto correlation function of the random noise process at different stages. With this analysis the receiver's output signal (frequency spectrum) is statistically characterized. With Matlab simulations, the analysis is verified and validated.

Next, the maximum range of the FMCW ranging system is analyzed, showing how the maximum range is affected.

Finally, a measure for the minimum range variation is provided by using the Cramer Rao Lower Bound and this is verified by simulations.

5.2 UWB FMCW Ranging Receiver

Figure 5.1 depicts the block diagram of the UWB FMCW receiver used for the investigation of the influence of noise on ranging. The purpose of discussing the receiver process is to introduce the different variables in a mathematical way and to discuss the different steps of the receiving process. The setup of the receiver is revealed by discussing the different steps of how the range information is retrieved from the received FMCW signal. This receiver principle is widely used in FMCW Radar applications as explained in [17].

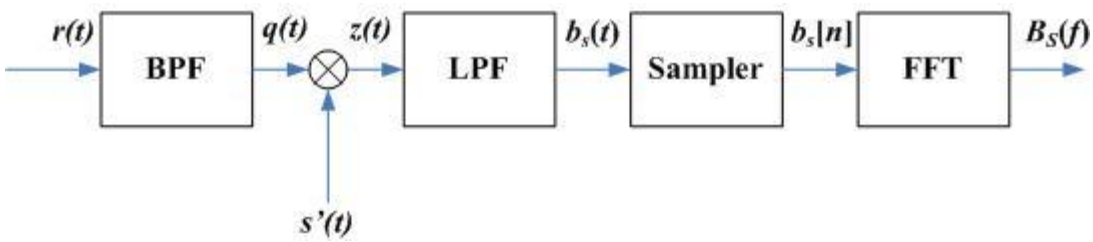

Figure 5.1 UWB FMCW receiver

In order to make figure 5.1 more realistic, Table 5.1 provides an example of UWB FMCW system design parameters. These parameters will be used for analysis and simulations.

Description	Variable	Value
Sweep duration period of the UWB FMCW signal	T	1ms
Sweep repetition frequency of the transmitted UWB FMCW signal	SRF	1KHz
Center frequency of the UWB FMCW signal and of the Ideal Band Pass Filter (which is matched to the UWB FMCW signal)	f_c	4GHz (λ=0.075 m)
Bandwidth of the UWB FMCW signal	B_{FMCW}	1GHz
Bandwidth of the ideal Band Pass Filter which is matched to the UWB FMCW signal	B_{BPF}	1GHz
Bandwidth of the ideal Low Pass Filter	B_{LPF}	5MHz
Standard room temperature of the UWB FMCW receiver	T_0	290 K
Noise figure of the UWB FMCW receiver	F	3.16 (5dB)

Table 5.1 UWB FMCW system parameters

The receiver setup is as follows. The UWB FMCW signal $s(t)$ is given by eq. (4.4). In the presence of noise this received signal can be written as:

$$r(t) = s(t) \otimes h(t) + n(t), \tag{5.1}$$

where $h(t)$ is the wireless channel impulse response. The noise is given by $n(t)$. Here $n(t)$ is a stationary zero mean Gaussian process, with its double sided $PSD_n(f)$ given by [20]:

$$PSD_n(f) = \tfrac{N_0}{2} = \tfrac{kT_{RX}}{2} \text{ [W/Hz]}, \tag{5.2}$$

where k is the Boltzmann's constant ($1.38 \cdot 10^{-23}$ J/K), T_{RX} is the equivalent input noise temperature of the receiver system in Kelvin.

The BPF output $q(t)$.

$r(t)$ is applied to an ideal BPF (with bandwidth $2W_b$) which is matched to the UWB FCMW signal. This BPF, as depicted in figure 5.2, only allows signals to pass which are within the frequency band of $s(t)$. Therefore, the BPF has the same bandwidth and center frequency as $s(t)$. In case of eq. (5.1), $s(t) \otimes h(t)$ is allowed to pass and $n(t)$ is filtered.

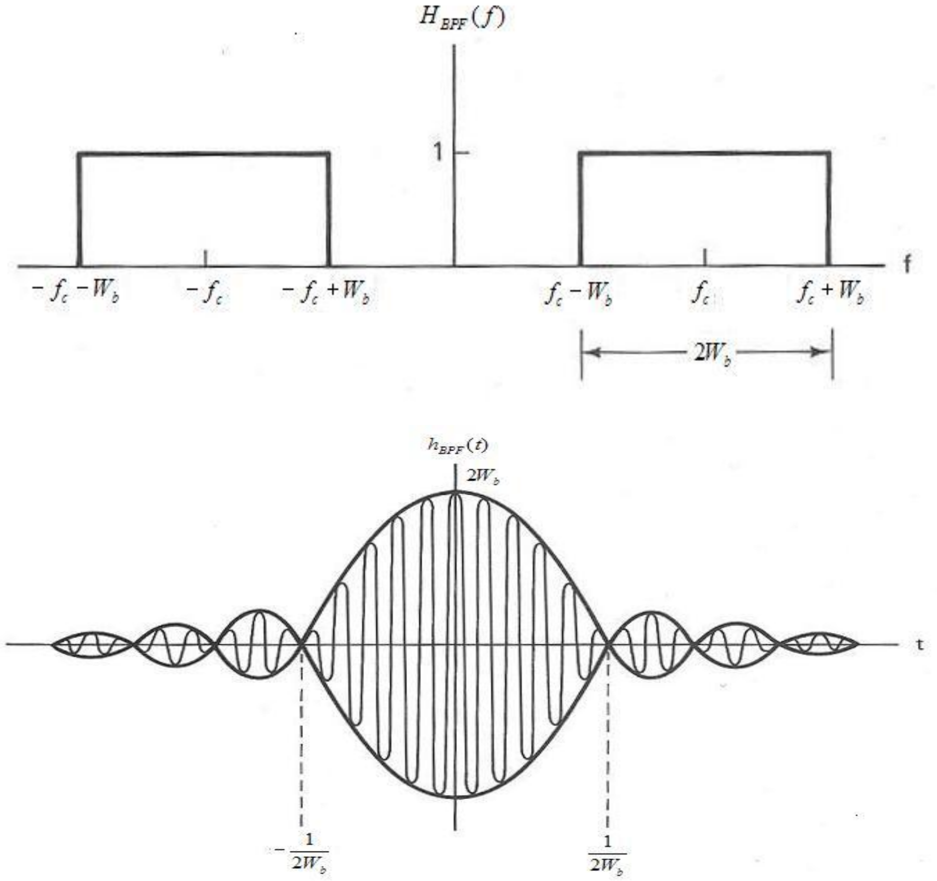

Figure 5.2 Ideal BPF [19]

The output $q(t)$ of the BPF is given by:

$$q(t) = \;\; s(t) \otimes h(t) + n(t) \;\; \otimes h_{BPF}(t) = \;\; \sum_{n=1}^{N} a_n s(t - \tau_n) + n(t) \;\; \otimes h_{BPF}(t), \tag{5.3}$$

where $s(t) \otimes h(t)$ is written as eq. (4.16) and the BPF impulse response $h_{BPF}(t)$ is given by:

$$h_{BPF}(t) = 2W_b \operatorname{sinc}(2W_b t) \cos 2\pi f_c t \tag{5.4}$$

The index b relates to the BPF and f_c is the center frequency. The Fourier Transform of $h_{BPF}(t)$ is $H_{BPF}(f)$ and is given by:

$$H_{BPF}(f) = \operatorname{rect}\left(\frac{f - f_c}{2W_b}\right) + \operatorname{rect}\left(\frac{f + f_c}{2W_b}\right) \tag{5.5}$$

Focusing only on the noise, the ideal BPF only allows noise to pass which is within the BPF bandwidth. This results in a stochastic process with a bandwidth of $2W_b$, a centre frequency of f_c and with its original noise PSD. This bandpass noise process can be presented by:

$$n(t) = \Re\{g_n(t) e^{j w_c t}\}, \tag{5.6}$$

where $g_n(t)$ is the complex envelope of the noise process centered around $\omega_c = 2\pi f_c$. Parameter $g_n(t)$ can be written as:

$$g_n(t) = n_x(t) + jn_y(t), \tag{5.7}$$

where the real random processes $n_x(t)$ and $n_y(t)$ are respectively, the in-phase and quadrature-phase components of the complex noise process and $j = \sqrt{-1}$. Both are independent processes with zero mean and equal variances. Because $n(t)$ is Gaussian, $n_x(t)$ and $n_y(t)$ are jointly Gaussian. Substituting eq. (5.7) in eq. (5.6) shows that the bandpass noise process is given by:

$$n(t) = n_x(t)\cos(\omega_c t) - n_y(t)\sin(\omega_c t) \tag{5.8}$$

The multiplication of $q(t)$ with the reference signal $s'(t)$.

This step of the receiver introduces the multiplication of the filtered signal $q(t)$ with the reference signal $s'(t)$, resulting in $z(t)$, given by:

$$\begin{aligned} z(t) &= q(t)s'(t) \\ &= \left(\sum_{n=1}^{N} a_n s(t-\tau_n)s'(t) + n(t) \;\; \otimes h_{BPF}(t) \right) s'(t), \end{aligned} \tag{5.9}$$

where $s'(t)$ is a replica of the original transmitted UWB FMCW signal $s(t)$. Multiplying an UWB FMCW signal with a replica of itself is performed to obtain the frequency difference between the two signals.

The signal and noise can be treated separately, because they are independent. For that part of eq. (5.9) that contains the UWB FMCW signal, $\sum_{n=1}^{N} a_n s(t-\tau_n)s'(t)$ shows a multiplication of two cosine functions resulting in a frequency sum term and a frequency difference term (according to eq. (4.8)) . The frequency difference term, as given by eq. (4.10), results in a baseband signal and the frequency sum term, as given by (eq. 4.9), results in a bandpass signal starting at $\geq 2f_l$. The bandpass noise process is also shifted to baseband and to a bandpass component with much higher start frequency.

The LPF output $b_s(t)$.

This step performs the baseband filtering of $z(t)$ by applying a LPF and limits the noise power contribution. $z(t)$ is applied to an ideal LPF resulting in $b_s(t)$. This is given by:

$$
\begin{aligned}
b_s(t) &= z(t) \otimes h_{LPF}(t), \\
&= (\sum_{n=1}^{N} a_n s(t-\tau_n) s'(t)) \otimes h_{LPF}(t) + ((n(t) \otimes h_{BPF}(t)) s'(t)) \otimes h_{LPF}(t),
\end{aligned}
\quad (5.10)
$$

where the LPF impulse response $h_{LPF}(t)$ is given by:

$$
h_{LPF}(t) = 2W_l \operatorname{sinc}(2W_l t), \quad (5.11)
$$

where W_l is the bandwidth and the index l relates to the LPF. The Fourier Transform of $h_{LPF}(t)$ is $H_{LPF}(f)$ and is given by:

$$
H_{LPF}(f) = \operatorname{rect}(\frac{f}{2W_l}) \text{ [Hz]}, \quad (5.12)
$$

Figure 5.3 depicts the ideal LPF.

We are only interested in the frequency difference component of the multiplication of the received signal and the replica of the transmitted signal. In case of the UWB FMCW signal, this part is expected to contain the beat frequency. The LPF allows only the baseband stochastic process to pass with frequencies up to its cut-off frequency. So, eq. (5.9) is then written as:

$$
\begin{aligned}
b_s(t) &= b_{s_{FMCW}}(t) + b_{s_{noise}}(t), \\
&= b_{s_{FMCW}}(t) + ((n(t) \otimes h_{BPF}(t)) s'(t)) \otimes h_{LPF}(t),
\end{aligned}
\quad (5.13)
$$

where $b_{s_{FMCW}}(t)$ is the beat signal due to the received UWB FMCW signal and $b_{s_{noise}}(t)$ is the contribution due to noise.

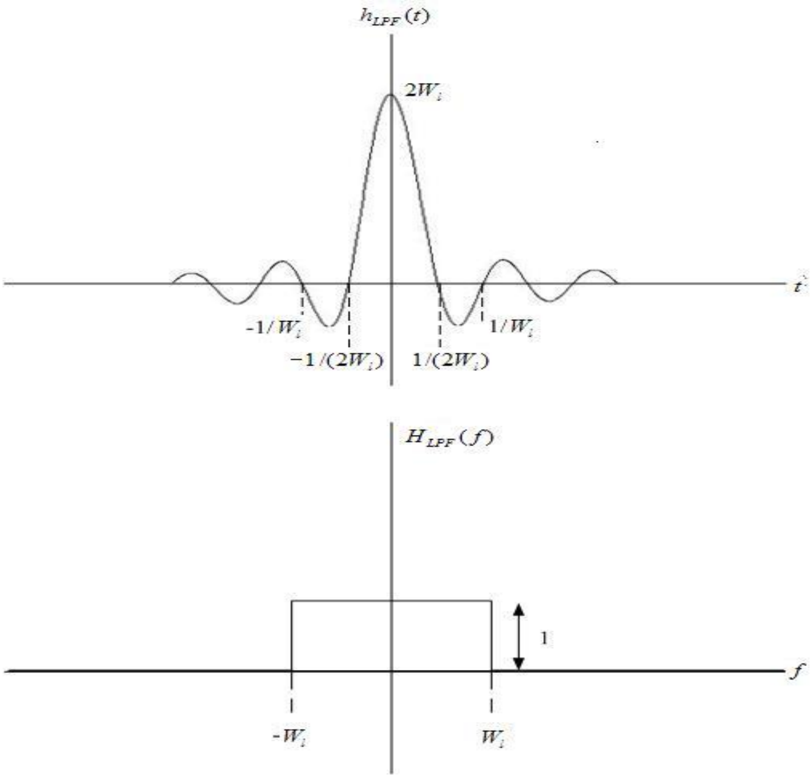

Figure 5.3 Ideal LPF [20]

Sampling $b_s(t)$.

In this step $b_s(t)$ is sampled. This is given by:

$$b_s[n] = b_s(t)\sum_{i=0}^{I}\delta(t - iT_{sample}) = b_s(iT_{sample}), \tag{5.14}$$

where i represents the sample number and T_{sample} represents the sampling period. In case of UWB FMCW signals, the maximum allowed beat frequency is derived from the maximum allowed (design parameter) propagation time delay. From this maximum beat frequency the sample frequency is derived. The discrete time signal is the input to the FFT.

The frequency spectrum of $b_s(t)$.

This step applies the FFT to $b_s[n]$ (which is given by eq. (5.15)) and presents the frequency spectrum of the noise corrupted UWB FMCW signal $b_s(t)$.

$$\begin{aligned} B_S(f) &= \mathscr{F}\ \ b_s[n]\ \ = \mathscr{F}\{b_{s\_FMCW}[n]\} + \mathscr{F}\{b_{s\_noise}[n]\}, \\ &= B_{s\_FMCW}(f) + B_{s\_noise}(f) \end{aligned} \tag{5.15}$$

This is a complex function of frequency and may be decomposed into two real functions, orthogonal to each other. This is given by:

$$\begin{aligned} B_s(f) &= (B_{s_X}(f) + jB_{s_Y}(f)) = \\ &= (B_{x\_FMCW}(f) + jB_{y\_FMCW}(f)) + (B_{x\_noise}(f) + jB_{y\_noise}(f)), \end{aligned} \tag{5.16}$$

where $B_{x\_FMCW}(f)$ and $B_{x\_noise}(f)$ represents the in-phase frequency component and $B_{y\_FMCW}(f)$ and $B_{y\_noise}(f)$ represents the quadrature-phase frequency component of the noise corrupted UWB FMCW signal. Depending on the amplitude of the frequency components of the noise process, the UWB FMCW frequency components are more or less distorted.

In case of an UWB FMCW signal without the presence of noise, the frequency spectrum of the receiver's output signal is a sinc pulse (due to the rectangular envelope of the transmitted UWB FMCW signal). The frequency component with the highest amplitude represents the beat frequency.

In the presence of noise, the FMCW frequency components are added with the frequency components of the noise process (of which the amplitudes are Gaussian distributed). This results in increased or decreased amplitudes of the frequency components. Due to this addition, a frequency component other than the beat frequency can have the highest amplitude and therefore be the ‘new’ beat frequency. This deviation of the true beat frequency is a measure for the range error.

5.3 Noise Analysis

Noise is described by its statistical properties. By calculating the ACF of the noise at the receiver output, information about the process being stationary or not and about its average power and power spectral density is retrieved. These characteristics show how noise contributes to the beat frequency of a received UWB FMCW signal.

This paragraph discusses the analysis of the autocorrelation function of the receiver’s output signal, the effect of FFT on the output power, the maximum range and the range estimation and range errors.

5.3.1 Analysis of the autocorrelation function of the Output Signal

The UWB FMCW receiver is further analyzed by calculating the auto correlation function of the random noise process. With this analysis the receiver’s output (frequency spectrum) is statistically characterized. Here the ACF is calculated for different steps of the receiving process. The ACF for a stochastic process ([21]) is given by,

$$R_x(t_1,t_2) = E[x(t_1)x(t_2)] \tag{5.17}$$

in case of stationary processes,

$$R_x(\tau) = E[x(t)x(t+\tau)] \tag{5.18}$$

where $\tau = t_1 - t_2$ is the time delay between the two processes. The relation between the PSD (Power Spectral Density) and the ACF in case of stationary processes [21] is given by,

$$PSD_x\left(f\right) = \mathscr{F}\left(R_x(\tau)\right) \tag{5.19}$$

The autocorrelation of the input signal $r(t)$ is given by:

$$\begin{aligned} R_r(t_1,t_2) &= E[r(t_1)r(t_2)], \\ &= E[(\sum_{n=1}^{N} a_n s(t-\tau_n) + (n(t)\otimes h_{BPF}(t)))(\sum_{n=1}^{N} a_n s(t+\tau-\tau_n) + (n(t+\tau)\otimes h_{BPF}(t+\tau))) \\ &= E[(\sum_{n=1}^{N} a_n s(t-\tau_n)\sum_{n=1}^{N} a_n s(t+\tau-\tau_n)] + R_n(\tau)\otimes h_{BPF}(\tau)\otimes h_{BPF}(-\tau) \end{aligned} \tag{5.20}$$

Appendix A shows the calculation of eq. (5.20).

For the calculation of the ACF at different stages of the receiver process, the UWB FMCW signal and the noise process are treated separately, due to the fact that the signal and noise are independent and the operations of the receiver process are linear operations.

In the remaining part of this paragraph we focus only on the noise part of eq. (5.20), in order to describe its frequency spectrum.

The autocorrelation function of $n(t)$

To calculate $R_n(\tau)$, eq. (5.18) is used. $R_n(\tau)$ is given by:

$$R_n(\tau) = \mathscr{F}^{-1}\ PSD_n(f) \tag{5.21}$$

Because $n(t)$ is a stationary process, substituting (5.2) in (5.21), results in $R_n(\tau)$ given by,

$$R_n(\tau) = \mathscr{F}^{-1}\left\{\frac{N_0}{2}\right\} = \frac{N_0}{2}\delta(\tau) \tag{5.22}$$

The autocorrelation function of $q(t)$

$R_q(\tau)$ is calculated via the frequency-domain. Because the BPF is a linear time-invariant system (LTI), $q(t)$ is still a stationary process. The PSD of $q(t)$ is given by,

$$PSD_q(f) = PSD_n(f)\,\left|H_{BPF}(f)\right|^2 \text{ [W/Hz]}, \tag{5.23}$$

The amplitude of $H_{BPF}(f)$ is given by:

$$\left|H_{BPF}(f)\right| = 1, \qquad f_l \le |f| \le f_h \tag{5.24}$$

where f_l and f_h are, respectively, the lowest and highest frequency of $H_{BPF}(f)$ (and of the FMCW signal because the BPF is matched to the FMCW signal). Equation (5.23) can now be written as:

$$PSD_q(f) = PSD_n(f)\,\left|H_{BPF}(f)\right|^2 = \frac{N_0}{2}\left(\mathrm{rect}\left(\frac{f-f_c}{2W_b}\right) + \mathrm{rect}\left(\frac{f+f_c}{2W_b}\right)\right) \text{ [W/Hz]} \tag{5.25}$$

$R_q(\tau)$ is calculated by performing the inverse Fourier Transform of (5.25). This is given by:

$$R_q(\tau) = \frac{N_0}{2} 2W_b \mathrm{sinc}(2W_b\tau)\cos 2\pi f_c\tau \tag{5.26}$$

The autocorrelation function of $z(t)$

For the calculation of $R_z(t_1, t_2)$ eq. (5.17) is used, giving:

$$R_z(t_1,t_2) = E[z(t_1)z(t_2)] = E[q(t_1)s'(t_1)q(t_2)s'(t_2)] \tag{5.27}$$

The expectation operation $E[.]$ only applies to the stochastic process $q(t)$. Because $s'(t)$ is deterministic it can be put outside the expectation operation. This results in:

$$R_z(t_1,t_2) = E[q(t_1)q(t_2)]s'(t_1)s'(t_2), \tag{5.28}$$

for $\tau = t_1 - t_2$, $E[q(t_1)q(t_2)]$ is known as eq. (5.26). Substituting eq. (5.26) in eq. (5.28) results in:

$$\begin{gathered} R_z(t_1,t_2) = \frac{N_0}{2} 2W_b \mathrm{sinc}(2W_b(t_1 - t_2)) \cos 2\pi f_c (t_1 - t_2) \\ A \cos 2\pi (f_l t_1 + ½\zeta t_1^2) A \cos 2\pi (f_l t_2 + ½\zeta t_2^2) \end{gathered} \tag{5.29}$$

Because (5.29) contains a multiplication of cosines, the cosine rule eq. (4.8) is applied. This results in:

$$\begin{aligned} R_z(t_1,t_2) = \frac{A^2}{2}\frac{N_0}{2} W_b \mathrm{sinc}(2W_b(t_1 - t_2)) \ & \cos 2\pi ((f_c - f_l)(t_1 - t_2) - ½\zeta(t_1^2 - t_2^2)) + \\ & \cos 2\pi \ \ (f_c + f_l)(t_1 - t_2) + ½\zeta(t_1^2 - t_2^2) \ + \\ & \cos 2\pi \ \ f_c(t_1 - t_2) - f_l(t_1 + t_2) - ½\zeta(t_1^2 + t_2^2) \ + \\ & \cos 2\pi \ \ f_c(t_1 - t_2) + f_l(t_1 + t_2) + ½\zeta(t_1^2 + t_2^2) \end{aligned} \tag{5.30}$$

The bandwidth and the center frequencies of $s'(t)$ and $h_{BPF}(t)$ are the same. This means that:

$$f_l = f_c - W_b \ \text{[Hz]} \tag{5.31}$$

Substituting eq. (5.31) in eq. (5.30) results in:

$$\begin{aligned} R_z(t_1,t_2) = \frac{A^2}{2}\frac{N_0}{2} W_b \,\mathrm{sinc}(2W_b(t_1 - t_2)) \ & \cos 2\pi ((W_b t_1 - ½\zeta t_1^2) - (W_b t_2 - ½\zeta t_2^2)) + \\ & \cos 2\pi \ \ ((2 f_c - W_b)t_1 + ½\zeta t_1^2) - ((2 f_c - W_b)t_2 + ½\zeta t_2^2) \ + \\ & \cos 2\pi \ \ (W_b t_1 - ½\zeta t_1^2) - (\ 2 f_c - W_b \ \ t_2 + ½\zeta t_2^2)) \ + \\ & \cos 2\pi \ \ (\ 2 f_c - W_b \ \ t_1 + ½\zeta t_1^2) - (W_b t_2 - ½\zeta t_2^2) \end{aligned} \tag{5.32}$$

The key idea of stationary processes is that the statistical properties of these processes do not change with time. Thus, for multiple realizations of a process, the mean and variance are independent of time. In this analysis the multiplication of stochastic process $q(t)$ with time varying signal $s'(t)$ causes the stochastic process $z(t)$ to be dependent on time. For that reason $z(t)$ is not stationary anymore. Also eq. (5.32) shows that $R_z(t_1,t_2)$ not only depends on $t_1 - t_2$ but also on t_1 and t_2.

The autocorrelation function of $b_{s\_noise}(t)$

$R_z(t_1,t_2)$ is the ACF of a non-stationary process. Before calculating $R_{b_{s\_noise}}(t_1,t_2)$, the LPF is applied on both time variables. This is given by:

$$\begin{aligned}
R_{b_{s_noise}}(t_1,t_2) &= E[z(t_1)\otimes h_{LPF}(t_1)z(t_2)\otimes h_{LPF}(t_2)],\\
&= \int_{-\infty}^{\infty}\int_{-\infty}^{\infty} E[z(t_1-u)z(t_2-v)h_{LPF}(u)h_{LPF}(v)]dudv,\\
&= \int_{-\infty}^{\infty} h_{LPF}(u)\int_{-\infty}^{\infty} E[z(t_1-u)z(t_2-v)h_{LPF}(v)dv]du,\\
&= \int_{-\infty}^{\infty} h_{LPF}(u)\int_{-\infty}^{\infty} R_z((t_1-u),(t_2-v))h_{LPF}(v)dv]du
\end{aligned} \tag{5.33}$$

where $h_{LPF}(t)=h_{LPF}(t_1)=h_{LPF}(t_2)$. Equation (5.33) is very complex, especially because $z(t)$ is a non-stationary process. To the best of my knowledge, no literature supports or provides a way to calculate an equation similar as (5.33). In order to show what's the effect of the LPF, first the LPF is applied to $R_z((t_1-u),(t_2-v))$ for t_1 is constant and after that the LPF is applied to the outcome of the previous convolution operation but now for t_2 is constant. From a frequency perspective the (ideal) LPF operation allows only frequencies to pass below its cut-off frequency (which is equal to W_l). Evaluating eq. (5.32), shows that all cosine parts which contain frequencies higher than W_l are excluded and the remaining sinc and cosine terms are frequency limited by $|W_l|$. This results in:

$$\begin{aligned}
R_{b_{s_noise}}(t_1,t_2) = \frac{A^2}{2}\frac{N_0}{2}W_b\mathrm{sinc}(2W_l(t_1-t_2))[\cos 2\pi(W_l(t_1-t_2)+\tfrac{1}{2}\frac{2W_l}{T}(t_1^2-t_2^2))\\
+\cos 2\pi(W_lt_1-\tfrac{1}{2}\frac{2W_l}{T}t_1^2)+\cos 2\pi(-W_lt_2+\tfrac{1}{2}\frac{2W_l}{T}t_2^2)]
\end{aligned} \tag{5.34}$$

Here $b_{s\_noise}(t)$ is a process depending on t_1-t_2 and on t_1 and t_2.

The LTI operations of the receiving process do not change the distribution type, meaning that $b_{s\_noise}(t)$ is still a Gaussian random process but due to the multiplication with $s'(t)$ it's not white anymore. The calculation of the mean value of this Gaussian process is given by:

$$\begin{aligned}
&E[n(t)] = E[n(t+\tau)] = 0,\\
&E[q(t)] = E[n(t)\otimes h_{BPF}(t)] = E[\int_{-\infty}^{\infty} n(t-u)h_{BPF}(u)du] =\\
&\qquad = E[n(t-u)]\int_{-\infty}^{\infty} h_{BPF}(u)du = E[n(t)]\int_{-\infty}^{\infty} h_{BPF}(u)du = 0,\\
&E[z(t)] = E[q(t)]s'(t) = 0\\
&E[b_{s_noise}(t)] = E[z(t)\otimes h_{LPF}(t)] = E[z(t)]\int_{-\infty}^{\infty} h_{LPF}(u)du = 0,
\end{aligned} \tag{5.35}$$

5.3.2 The Statistical Characterization of $B_{s\_noise}(f)$

Once the random process $b_{s\_noise}(t)$ is statistically characterized, the statistical characteristics of $B_{s\_noise}(f)$ can be derived. Due to the linear operations of the receiver process, the type of distribution of the amplitude of the (intermediate) signals does not change. $n(t)$ is a Gaussian distributed process and therefore $B_{s\_noise}(f)$ is also Gaussian.

$b_{s\_noise}(t)$ is a bandpass noise process consisting of in-phase and quadrature-phase components. The quadrature Fourier series of $b_{s\_noise}(t)$ results in a complex valued $B_{s\_noise}(f)$ as given by eq. (5.16) [20]. Reference [22] shows that when a zero mean Gaussian distributed process is applied to a FFT, the output is also zero mean Gaussian and that the standard deviation of the Gaussian process is inversely related to the standard deviation of its Fourier transform. In physical terms, the narrower in time a pulse is, the greater the spread of frequency components it contains.

In the case when only noise is present, the Fourier transform of the bandpass noise process is decomposed in two orthogonal real functions $B_{x\_noise}(f)$ and $B_{y\_noise}(f)$. Because $B_{s\_noise}(f)$ is Gaussian, $B_{x\_noise}(f)$ and $B_{y\_noise}(f)$ are two jointly Gaussian processes, each with equal mean and variance. Reference [23] shows that the magnitude of a complex valued random process, consisting of two orthogonal Gaussian processes, is a Rayleigh distributed process if both orthogonal processes have the same mean and standard deviation. $B_{s\_noise}(f)$ corresponds to this theory and hence $\left|B_{s\_noise}(f)\right|$ is a Rayleigh distributed process (with mean $\sqrt{\frac{\pi}{2}}\sigma$ and variance $(2-\frac{\pi}{2})\sigma^2$ where σ equals that of its Gaussian components). The variance and mean are not independent as in a Gaussian distribution.

In case of an UWB FMCW signal in the presence of noise, $B_s(f)$ consists of the summation of the real parts and the summation of the imaginary part of the UWB FMCW signal and the noise process as given by eq. (5.36).

$$B_s(f) = (B_{x\_FMCW}(f) + B_{x\_noise}(f)) + j(B_{y\_FMCW}(f) + B_{y\_noise}(f)) \tag{5.36}$$

According to [16] this results in $|B_s(f)|$ being Rician distributed. The Rician distribution is given by:

$$p_{rician}(x) = \frac{x}{\sigma^2}\exp(-\frac{x^2+a^2}{2\sigma^2})I_0(\frac{xa}{\sigma^2}), \tag{5.37}$$

where x represents the amplitude of the noise corrupted signal, a represents the (fixed) amplitude of the FMCW frequency components, σ is the standard deviation and I_0 is the zero-order modified Bessel function.

To retrieve the beat frequency from the PSD of the noise corrupted $B_s(f)$, the frequency component with maximum amplitude is estimated, for instance, by use of the Maximum Likelihood Estimator (MLE). This is given by:

$$\hat{f}_b = \arg\max_f |B_s(f)|^2 \tag{5.38}$$

The difference between the actual (noise free) beat frequency and the estimated beat frequency (frequency with maximum amplitude) of the Rician distributed $|B_s(f)|$, results in a beat frequency error. The range error, due to the frequency error, is given by:

$$\Delta R = \frac{cT}{B}(f_b - \hat{f}_b) \tag{5.39}$$

For small signal to noise ratio's, the contribution of noise influences the sinc pulse of $|B_{s\_FMCW}(f)|$ in such way that a maximum occurs at a slightly different (beat) frequency. For high signal to noise ratio's, this contribution is very small and hardly influences the sinc pulse.

5.3.3 The SNR after Application of the FFT

The FFT operation operates on an input signal of a specific time period. The FFT considers the signal of this observation to be periodic. When the start and end points of the observed signal are not the same, discontinuities occur at the transition from the current period to the following period. This is depicted in figure 5.4.

In the frequency domain, these discontinuities introduce high frequency components. When this signal is transformed from the time domain to the frequency domain, the signal's total energy is 'smeared' over its true frequency components (the frequency components of the actual signal) and over the high frequency components due to the discontinuities. Thus, from the signal's total energy, a part of the energy is placed at the high frequency components and less energy remains for the true frequency components. The amplitude representation of the signal's frequency components after the FFT operation is less than the actual amplitude of the signal but the total energy is the same. This smearing of energy of the true frequencies into adjacent frequencies is called leakage.

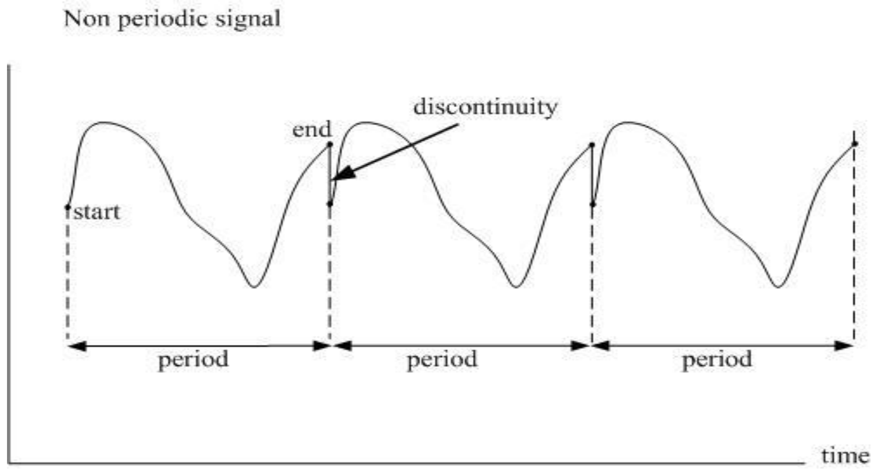

Figure 5.4 Periodic signal with fast changes

To reduce this smearing of energy and preserve the amplitude of the signal, windowing is used. The principle of windowing is, weighting the observed signal to smoothly reduce its boundaries (start and end point) to zero so that the windowed signal becomes periodic. Different window types are available for example, the Rectangular window, the Exponential window or the Hanning window. Windowing introduces loss of signal power. The reduction of signal power due to windowing is called the (In)Coherent Power Gain [24], [25] and [26].

Assume a windowed noise free sinusoid sampled with *N* samples. For every sample, the FFT adds a contribution to the (sinusoid) frequency component of the frequency spectrum. The summed contributions is called the peak signal gain. This means that the more samples are taken the higher the peak signal gain, resulting in a difference of signal input and output energy. This peak signal gain is corrected by normalizing to the number of samples. The normalized Coherent Signal Gain is given by:

$$\text{Coherent Signal Gain} = \frac{1}{N}\sum_{n=1}^{N} w[n], \tag{5.40}$$

where N is the number of samples and $w[n]$ is the weighting factor of the window at the corresponding samples. This weighting factor will be multiplied with the actual amplitude.

For the signal power the normalized Coherent Power Gain is given by:

$$\text{Coherent Power Gain} = \left(\frac{1}{N}\sum_{n=1}^{N} w[n]\right)^2 \tag{5.41}$$

When noise is fed into the FFT, the gain due to the FFT is called the Incoherent Power Gain. From the noise power perspective, where the noise power is given by σ_{noise}^2, the accumulated noise power due to N weighted samples is given by:

$$\text{Accumulated Noise Power } = \sigma_{noise}^2 \sum_{\mathrm{n=1}}^{\mathrm{N}} \mathrm{w[n]}^2 \tag{5.42}$$

The normalized Incoherent power Gain is then given by:

$$\text{Incoherent Power Gain} = \frac{1}{N} \sum_{\mathrm{n=1}}^{\mathrm{N}} \mathrm{w[n]}^2 \tag{5.43}$$

The ratio of the Coherent Power Gain and the Incoherent Power Gain is called the Processing Gain and is given by:

$$\text{Processing Gain} = \frac{\left(\frac{1}{N} \sum_{\mathrm{n=1}}^{\mathrm{N}} \mathrm{w[n]}\right)^2}{\frac{1}{N} \sum_{\mathrm{n=1}}^{\mathrm{N}} \mathrm{w[n]}^2} \tag{5.44}$$

For a *rectangular window* with an amplitude of one (similar as no windowing), the value of all the $\mathrm{w[n]}$ samples is one, then the Processing Gain becomes 1.

For other types of window, the Processing Gain is reduced (less than 1) due to the fact that the window ‘forces’ the start and end values of the signal to go smoothly to zero according to a certain window wave form. Reference [26] elaborates more on the different types of windows and the corresponding (In) Coherent Power Gain.

In the case of ranging with an UWB FMCW signal with a rectangular envelope, the effect of the FFT is an unity Processing Gain.

5.3.4 Maximum Range

For calculating the maximum range of the UWB FMCW ranging system, the signal to noise ratio is used. This is given by:

$$SNR = \frac{P_r}{P_n}, \tag{5.45}$$

where P_r is the received signal power and P_n is the thermal noise power. The thermal noise power of a stationary process is related to $R_n(0)$.

For calculating the maximum range, the SNR of the signal after the LPF is required. This signal represents the power of the beat signal and the available noise power (due to the LPF bandwidth). SNR_{LPF} represents the SNR after the LPF and SNR_{BPF} represents the SNR after the BPF. Because after the LPF less noise power is admitted, the SNR_{LPF} is higher than SNR_{BPF} .The ratio between SNR_{LPF} and SNR_{BPF} is the SNR gain given by:

$$G_{SNR} = \frac{SNR_{LPF}}{SNR_{BPF}} = \frac{B_{BPF}}{B_{LPF}} \tag{5.46}$$

Appendix B explains the calculation of G_{SNR} .

The Noise Power after the BPF

According to [20], P_n is described as:

$$P_n = kT_{system}B \text{ [W]}, \tag{5.47}$$

where B is the bandwidth equal to the LPF bandwidth, k is the Boltzmann's constant (5.2) and T_{system} is the receiver system noise temperature (in Kelvin) which depends on the noise figure (NF) F of the UWB receiver. References [27], [28] and [29] show that for UWB receivers with a Low Noise Amplifiers (LNA), a F=5 dB in the frequency range 3.1-10.6 GHz is a reasonable value, which value we assume here. The receiver system temperature is then given by:

$$T_{system} = T_0(F-1) = 290\text{K}(3.16\text{-}1) \approx 626\text{K}, \tag{5.48}$$

where T_0 is the standard room temperature (290K). Then kT_{system} is calculated to be -171dBm/Hz.
P_n in dB is then given by:

$$P_n = -171\,[\text{dBm/Hz}] + 10\log_{10} B\,[\text{Hz}] \tag{5.49}$$

The Received Power

According to Friis Transmission Equation, P_r is given by:

$$P_r = P_t G_t G_r G_{fs} = P_t G_t G_r \left(\frac{\lambda}{4\pi R}\right)^2 \text{ [W]}, \tag{5.50}$$

where the path loss exponent $\eta = 2$, λ corresponds to the wavelength of the center frequency of the signal and the distance between transmitter and receiver is R.

The maximum transmit power $P_{t_{MAX}}$, of the UWB signal, is subjected to the FCC regulations [4]. From [10] and [30] we know that, the FCC limits the UWB emissions in terms of peak power and average power. The transmitted peak power should be less than 0dBm when measured with a spectrum analyzer in any 50MHz bandwidth used by the signal. This is given by:

$$P_{t_{MAX}} \leq 0.001\left(\frac{B}{50\cdot 10^{6}}\right)^{2} \;\; [\mathrm{W}] \tag{5.51}$$

The average transmitted power spectral density should be less than $-41.25\mathrm{dBm/MHz}$ in any 1 MHz bandwidth used by the signal. This is given by:

$$P_{average} \leq 75\mathrm{nW} \text{ in any 1MHz bandwidth} \tag{5.52}$$

The Sweep Repetition Period (SRP) of the FMCW signal equals T_{sweep} (which is assumed $1\mathrm{ms}$) causing a continuous transmission. The Sweep Repetition Frequency (SRF) is given by:

$$SRF = \frac{1}{SRP} = \frac{1}{1\text{ ms}} = 1\text{ KHz} \tag{5.53}$$

Because of the continuous signal transmission of the UWB FMCW signal, only the average power is relevant for the power indication. From the FCC point of view, the maximum transmit power is dominated by the $P_{average}$ restriction of the FCC power regulation. This is given by:

$$P_{t_{MAX}} \leq 75\cdot 10^{-9}\left(\frac{B}{SRF}\right)^{2} \;\; [\mathrm{W}] \tag{5.54}$$

Which FCC power restriction is valid for FMCW signals? As described by reference [30] (for pulse based ranging) when the signal's pulse repetition frequency is larger than the 1MHz measurement resolution bandwidth, the 1MHz resolution bandwidth filter receives the following (input) pulse before the output has died out. The higher the input pulse frequency, the more constant the output. From the output perspective, it seems that there is a constant input signal present, so its duty cycle is approximately one. This output perspective can also be translated into an input signal which is equal to a continuous wave signal. This means that not the peak power, but the average power is relevant for the power indication. Therefore, the FCC average power constrain is applied. Thus, for UWB FMCW signals also the FCC average power constraint is used.

In case of isotropic radiating transmit and receive antennas, P_r is given by:

$$P_r = P_{t_{MAX}}\left(\frac{\lambda}{4\pi R}\right)^{2} \leq 75\cdot 10^{-9}\left(\frac{B}{SRF}\right)^{2}\left(\frac{\lambda}{4\pi R}\right)^{2} \;\; [\mathrm{W}] \tag{5.55}$$

The maximum range the system can cover, depends on the minimum required SNR. Combining eq. (5.45), (5.47), (5.48) and (5.55) results in the derived maximum range R, assuming $G_t = G_r = 1$. The maximum range, based on the received beat signal is given by:

$$R \leq \frac{\lambda}{4\pi SRF}\sqrt{\frac{75\cdot 10^{-9} B_{LPF}}{SNR_{LPF} k T_0 (F-1)}} \;\; [\mathrm{m}] \tag{5.56}$$

For an UWB FMCW system with parameters given by Table 5.1 and, for example, an $SNR_{BPF} = 100$ and a G_{SNR} according to eq. (5.46), the maximum range based on the received beat signal is $R \leq 278$ m. According to eq. (5.52), the UWB FMCW system with 1GHz Bandwidth has a $P_{average} \leq 75\mu\text{W}$, transmitted over a 1ms period. This means an energy of $75mJ$ for every second.

If we compare this to an UWB pulse based ranging system with similar parameters, the peak power FCC restriction dominates the $P_{t_{MAX}}$ limit. In this case $P_{t_{MAX}} \leq 0.4\text{W}$ according to eq. (5.51). For a system with a pulse width of 1ns ($\approx 1/B$) and a Pulse Repetition interval (PRI) of 1ms ($= 1/SRF$), every second $0.4\mu\text{J}$ of energy is transmitted. The maximum range R is then given by:

$$R \leq \frac{\lambda}{4\pi 50 \cdot 10^6} \sqrt{\frac{0.001B}{SNR_{BPF} k T_0 (F-1)}} \text{ [m]} \tag{5.57}$$

Applying the same parameter values of Table 5.1 to eq. (5.57), results in a maximum range value of $R \leq 128$ m.

For UWB pulse based ranging systems to have an equal maximum range, the peak power should be much larger, but this may violate the FCC power restriction. In that case, increasing the bandwidth is a solution, which implies a very small pulse width with even higher peak power. But the pulse width is fixed by the fixed value of the bandwidth. Eventually, only a small amount of energy is transmitted. Thus, the fixed value for the bandwidth and the FCC power restrictions causes the UWB pulse based ranging system to have a shorter maximum range than the UWB FMCW ranging system.

In case of the UWB FMCW ranging system, the large amount of received energy, positively affects the ranging performance. For indoor environments (short range), ranging with UWB FMCW is a very good solution.

5.3.5 Range Errors

Estimating the beat frequency $\hat{f}_b$ from the frequency spectrum of a noisy beat signal $B_S(f)$, introduces frequency errors which result in range errors. If the SNR is large, the range error is small. In every estimation process there is a lower bound on the variance of the estimated variable. The more accurate the estimation process, the lower the minimum bound. In the process of range estimation, the Cramer Rao Lower Bound (CRLB) is used to represent the minimum variance of the estimated range. References [31] and [32] present different CRLB's that can be used to calculate the minimum variance of the range estimation.

Reference [31] presents a CRLB for the ToA principle. This specifically holds for pulse based ranging. The estimated variable is the time delay a received pulse experiences during its propagation. The CRLB that shows the minimum range deviation based on the estimated delay time is given by:

$$\sqrt{Var[\hat{R}]} \geq \frac{c}{2\sqrt{2}\pi\sqrt{SNR}\beta_{ebw}}, \tag{5.58}$$

where $\hat{R}$ is the estimated distance from transmitter to receiver and β_{ebw} is the effective or rms (root mean square) bandwidth of the transmitted pulse. Equation (5.58) shows that the minimum range deviation is inversely proportional to the SNR and β_{ebw}. Thus, the higher the SNR and/or the larger the rms bandwidth (the smaller the transmitted pulse), the smaller the minimum range deviation.

Reference [32] presents the CRLB based on the frequency estimation. Here, a specific frequency is estimated from a received signal. This CRLB is valid for FMCW ranging. The CRLB that shows the minimum range deviation based on the estimated beat frequency is given by:

$$\sqrt{Var[\hat{R}]} \geq \frac{cT_{sweep}}{B_{FMCW}} \frac{\sqrt{6} f_{sample}}{2\pi\sqrt{SNR}N\sqrt{N}}, \tag{5.59}$$

where N is the number of time samples used for the observed signal and f_{sample} is the number of time samples per observation period. Equation (5.59) shows that the minimum range deviation is inversely proportional to the SNR and N. Thus, the higher the SNR and/or the larger the N, the smaller the minimum range deviation. Here N determines the frequency resolution of the estimation process. The larger N, the higher the resolution of the estimated frequency. This leads to more accurate estimation and thus to smaller minimum frequency deviation. Smaller minimum frequency deviation results in smaller minimum range deviation.

In case of FMCW ranging the CRLB for frequency estimation provides the (proper) minimum range deviation. The SNR from eq. (5.59) represents the SNR_{LPF}. Considering the CRLB for the delay time variable. In this case, the SNR from eq. (5.58) represents the SNR_{BPF} and the β_{ebw} represents the B_{FMCW}.

For $SNR_{BPF} = 1$ and $\beta_{ebw} = 1\text{GHz}$, the CRLB for ToA (eq. (5.58)) shows a minimum range deviation of $3.37 \cdot 10^{-3}$ m. In case of CRLB for frequency estimation, where $SNR_{LPF} = 200$,

$N = 20000$ and $f_{sample} = 2 \cdot 10^9 \text{Sa/s}$, eq. (5.59) shows a minimum range deviation of $5.84 \cdot 10^{-4}$ m. The minimum range deviation calculation for both CRLB's should be the same. Calculations show that both CRLB's differ a factor 5.8. Unfortunately, I am unable to explain what causes this factor of difference.

References [33], [34] and [35] indicate that, in case of MLE, the range deviations are identical to the CRLB at high SNR's. For low SNR's the range deviations increase rapidly above the CRLB and therefore the CRLB is not valid anymore.

For indoor UWB FMCW ranging, minimum variations in the order of a few cm is already a good (accurate) performance. This shows that the UWB FMCW techniques have good potential for indoor ranging applications.

5.4 Simulation and Validation

In this paragraph the noise analyses of paragraph 5.3 are simulated, verified and validated. Paragraph 5.4.1 provides the system parameters used for the simulations. Paragraph 5.4.2 verifies and validates the ACF analysis and Paragraph 5.4.3 verifies the statistical characterization and validates the range error deviation.

5.4.1 UWB FMCW System Parameters

To verify and/or validate the ACF analysis, the ACF process is simulated and the corresponding results are discussed. The FMCW system model, as depicted in figure 5.1, is implemented in Matlab. The applied UWB FMCW variables and their corresponding values are given by Table 5.2.

Variable name	Variable value(s)	Number of samples
AWGN noise $n(t)$	Stationary Gaussian process	N=2000
	$\mu = 0$	
	$\sigma = 1$	
	$0 \le t \le 1 \mu s$	
UWB FMCW signal $s(t)$, $s'(t)$	$A_t = A = 1\text{V}$	N=2000
	$f_l = 3.5\text{GHz}$	

	$2W_b = 1\text{GHz}$	
	$T_{sweep} = 1\text{ms}$	
	$0 \le t \le 1\mu s$	
BPF $h_{BPF}(t)$	$f_c = 4\text{GHz}$	N=4000
	$f_l = 3.5\text{GHz}$	
	$2W_b = 1\text{GHz}$	
	$-1\mu s \le t \le 1\mu s$	
LPF $h_{LPF}(t)$	$W_l = 5\text{MHz}$	N=4000
	$-1\mu s \le t \le 1\mu s$	
Maximum propagation delay time	$\tau_{\max} = 5\mu\text{s}$	

Table 5.2 UWB FMCW Simulation variable values

The maximum propagation delay time is set to $\tau_{\max} = 5\mu\text{s}$. In case of an indoor environment the average propagation delay (τ_d) is about $10-100\text{ns}$, therefore all contributing multipath components will be within the interval $0 < \tau_{\max} < 5\mu\text{s}$. Thus $T_{sweep} >> \tau_{\max} >> \tau_d$.

Substituting $\tau_{\max}$ in eq. (4.13) with system parameters $T_{sweep} = 1\text{ms}$ and $2W_b = 1\text{GHz}$, provides the maximum beat frequency $f_{b_{\max}} = 5\text{MHz}$ that is expected for $\tau_{\max} = 5\mu\text{s}$. The LPF bandwidth is designed to only allow beat frequencies up to $f_{b_{\max}}$ to pass the LPF. Thus the LPF bandwidth $W_l = 5\text{MHz}$. According to the Nyquist sampling theory (when sampling f_b), the sampling frequency f_{sample} should be chosen at least 10MHz.

For the simulations 100 iterations are performed.

5.4.2 Simulation and Verification of the Autocorrelation Function

For verification of the mathematical analysis of the autocorrelation function, we are mainly interested in the autocorrelation function of $b_{s\_noise}(t)$. This paragraph only shows the simulation results of those autocorrelation functions which introduce deviations or emphasize the findings from the theoretical analysis.

The autocorrelation function of $n(t)$

A noise realization is generated with a normal distribution as depicted in figure 5.5. The ACF of $n(t)$, as given by eq. (5.22), indicates that this is a Dirac delta function. This is depicted in figure 5.6. In theory, the noise has a frequency span up to infinity. For the simulation, a noise sample is created of limited time. This time limited noise sample introduces the noisy parts left and right from the pulse. When noise samples of unlimited time could be used, these noisy parts would be cancelled out to zero.

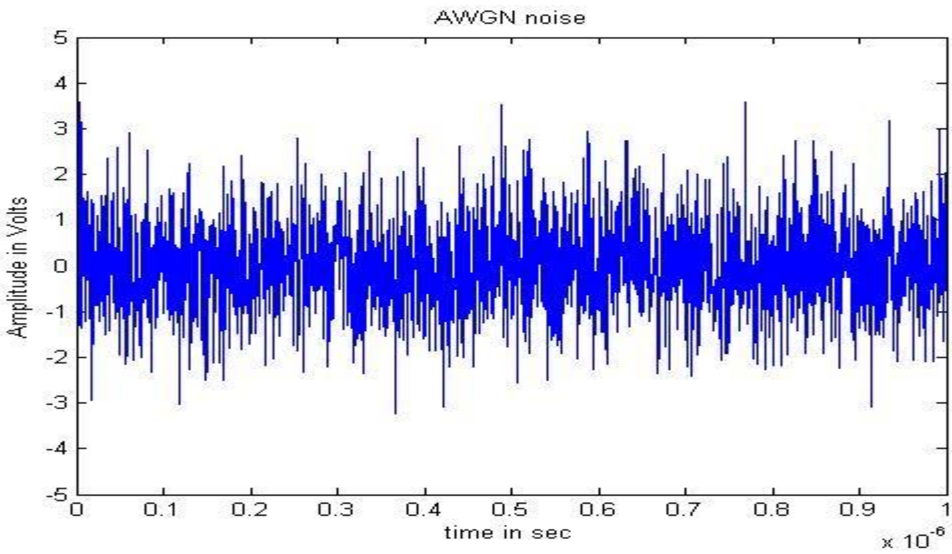

Figure 5.5 Noise realization

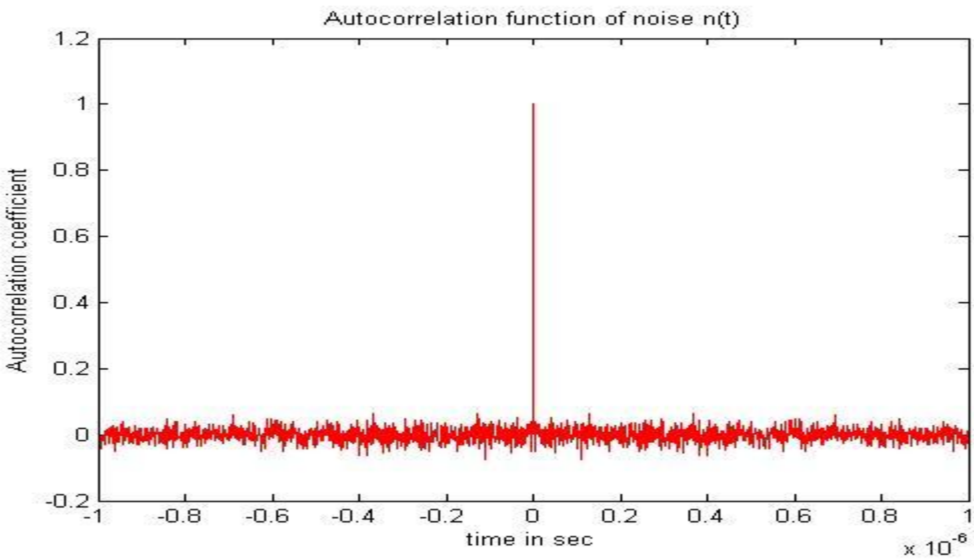

Figure 5.6 AWGN ACF

The autocorrelation function of $z(t)$

In the theoretical analysis of the ACF of $z(t)$, the multiplication of the stochastic process $q(t)$ with the time varying signal $s'(t)$ causes the stochastic process $z(t)$ to depend on time and not only on the time difference between two samples. For that reason $z(t)$ is not stationary anymore. This is also shown in eq. (5.32), where the different cosine terms are depending on $t_1 - t_2$ and on t_1 and t_2. Figure 5.7 depicts the ACF of $z(t)$. The horizontal plane consists of two time axis'. One axis representing t_1 and the other axis representing t_2 and the diagonal lines indicate the different time differences $(t_1 - t_2)$.

For stationary processes the ACF amplitude stays the same as long as $t_1 - t_2$ is constant (independent of the values of t_1 and t_2). Figure 5.7 shows that the main diagonal line from the ACF of $z(t)$ varies with time which indicates that $z(t)$ is non-stationary. The noisy parts left and right from the pulse are introduced due to the time limited noise sample. This is depicted in figure 5.8.

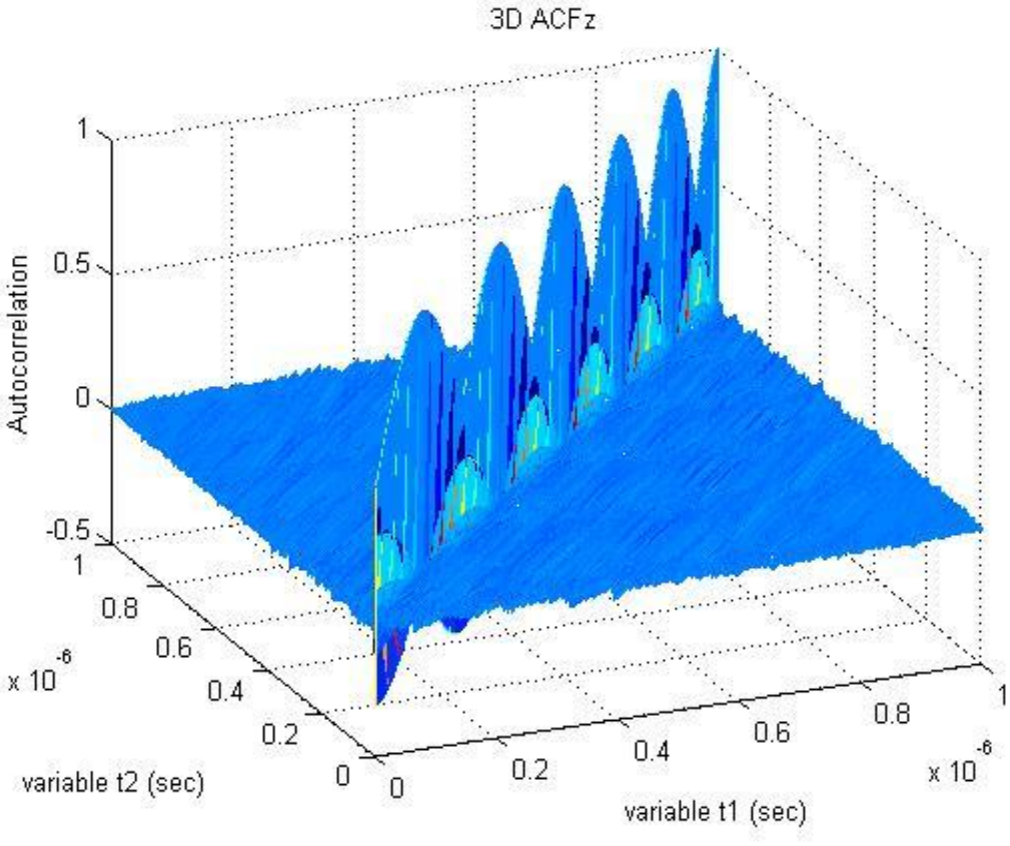

Figure 5.7 The ACF of the multiplier output signal

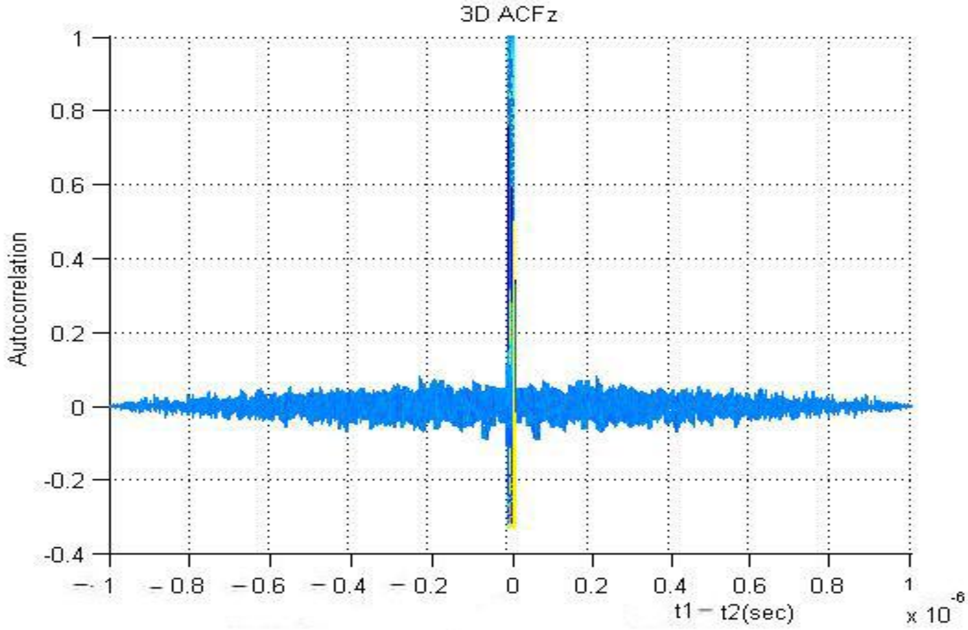

Figure 5.8 ACF of the multiplier output signal

The autocorrelation function of $b_{s\_noise}(t)$

Equation (5.34) shows the ACF of $b_{s\_noise}(t)$. $R_{b_{s\_noise}}(t_1,t_2)$ is simulated by performing a 2D convolution of the LPF and $R_z(t_1,t_2)$, averaged over 100 noise realizations. Figure 5.9 depicts the ACF of $b_{s\_noise}(t)$. In this figure the horizontal plane consists of two time axis'. One axis representing t_1 and the other axis representing t_2 and the diagonal lines indicate the different time differences $(t_1 - t_2)$.

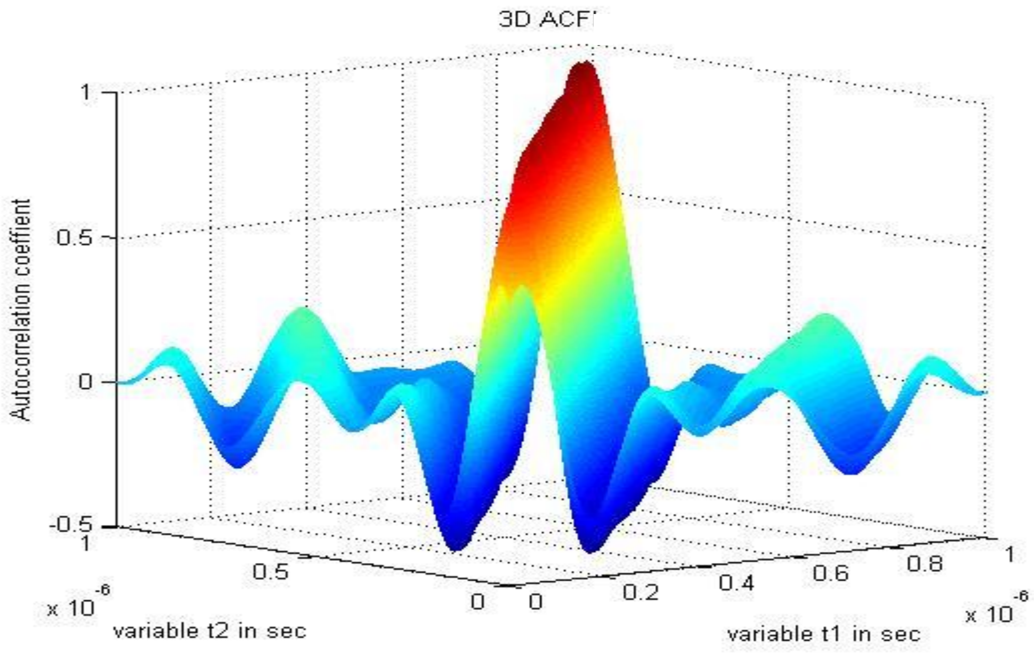

Figure 5.9 Sampled ACF of the LPF output based on 100 realizations

$b_{s\_noise}(t)$ is as sampled at the Nyquist rate ($f_{sample} = 2W_l$) which results in the ACF of $b_{s\_noise}[n]$. Sampling the ACF of $b_{s\_noise}(t)$ at the Nyquist rate is sampling the ACF at $t_1 - t_2 = 0$ and at the zero crossings. For $t_1 - t_2 = 0$, the sampled ACF results in the constant value $R_{b_{s\_noise}}(0) = a\frac{A^2}{2}N_0W_b$. Figure 5.10 depicts $R_{b_{s\_noise}}(0)$.

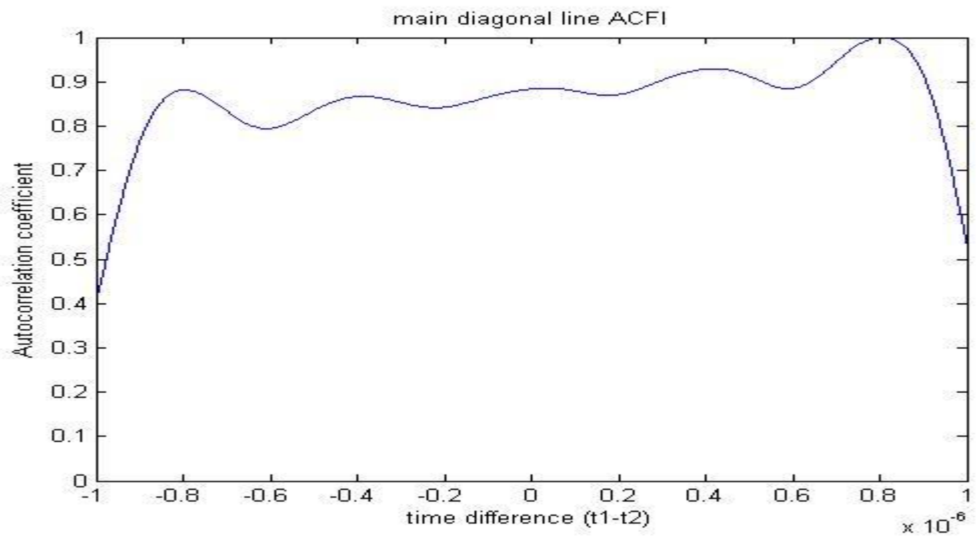

Figure 5.10 ACF of $b_{s\_noise}(t)$ for $t_1 - t_2 = 0$

Furthermore, sampling $R_{b_{s\_noise}}(t_1,t_2)$ at $t_1 - t_2 = u\frac{1}{2W_l}$ (for $u = 1,2,3,..N$) results in the value zero, because these samples are taken at the zero crossings. Substituting $t_1 - t_2 = u\frac{1}{2W_l}$ in eq. (5.34) results in a term $\mathrm{sinc}(u)$. This $\mathrm{sinc}(u)$ term is zero for every value of u and $u \neq 0$. This means that the ACF for $t_1 - t_2 = u\frac{1}{2W_l}$ is zero independent from t_1 and t_2. These samples are therefore uncorrelated. For all other values of t_1 and t_2 where $t_1 - t_2 \neq u\frac{1}{2W_l}$, they are correlated.

Simulation shows that samples taken at different zero crossings are zero and constant, meaning that the $b_{s\_noise}[n]$ is a stationary process. Therefore $B_{s\_noise}(f)$ is a stationary process. Figure 5.11, 5.12 and 5.13. depict the samples taken at the first, second and third zero-crossing and shows that the value for these samples is constant and should be zero.

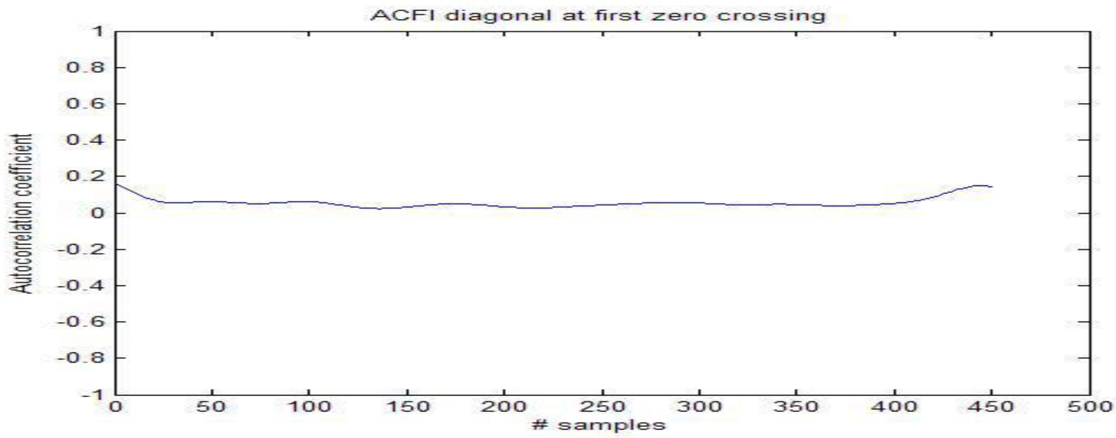

Figure 5.11 First ACF zero-crossing

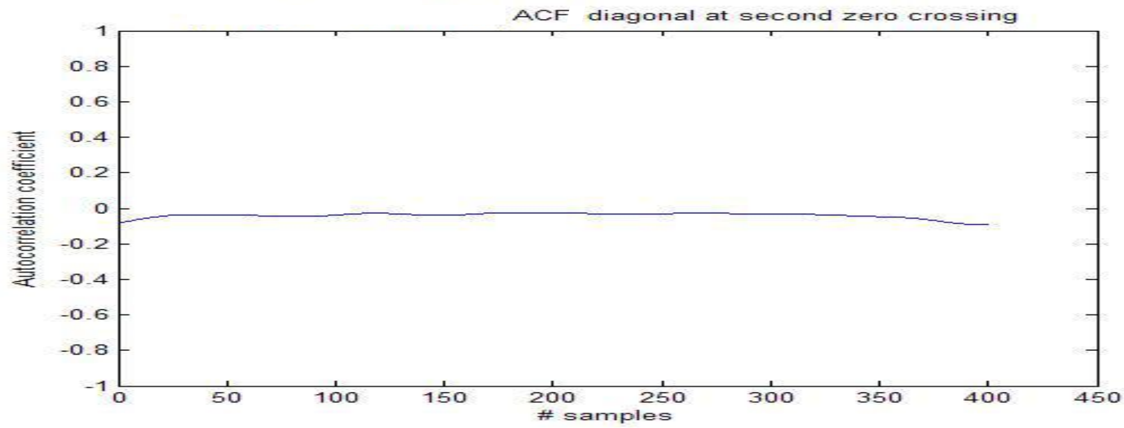

Figure 5.12 Second ACF zero-crossing

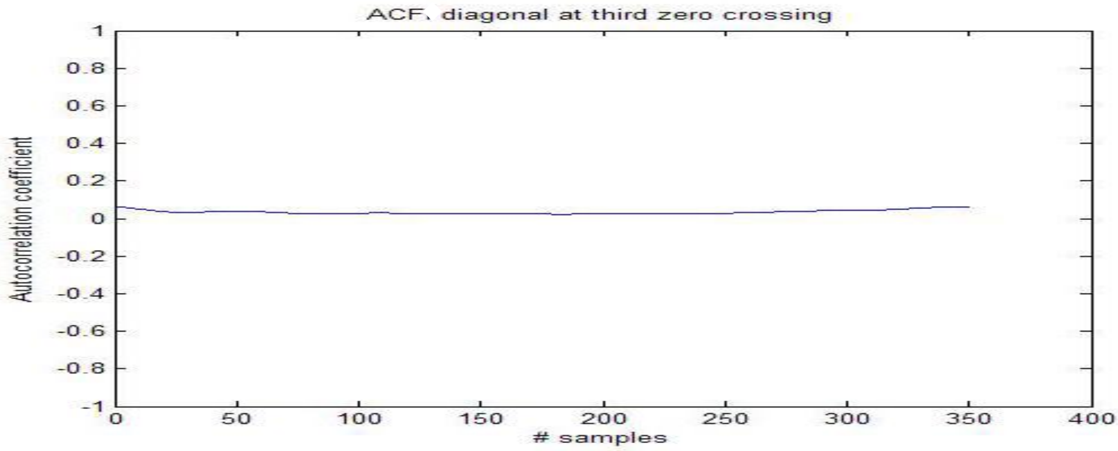

Figure 5.13 Third ACF zero-crossing

5.4.3 Verification of Statistical Character of $b_{s\_noise}(t)$ and $B_{s\_noise}(f)$

In this paragraph the statistics of $b_{s\_noise}(t)$ and $B_{s\_noise}(f)$ are verified. A simulated noise process with unit variance (presented by figure 5.5) is used to simulate the LPF output $b_{s\_noise}(t)$. This is depicted in figure 5.14. The amplitude distribution of this process is depicted in figure 5.15. Calculations from this amplitude distribution show that $b_{s\_noise}(t)$ has a zero mean and a certain standard deviation. With the Matlab operation 'Lillietest' it is checked whether $b_{s\_noise}(t)$ is Gaussian distributed.

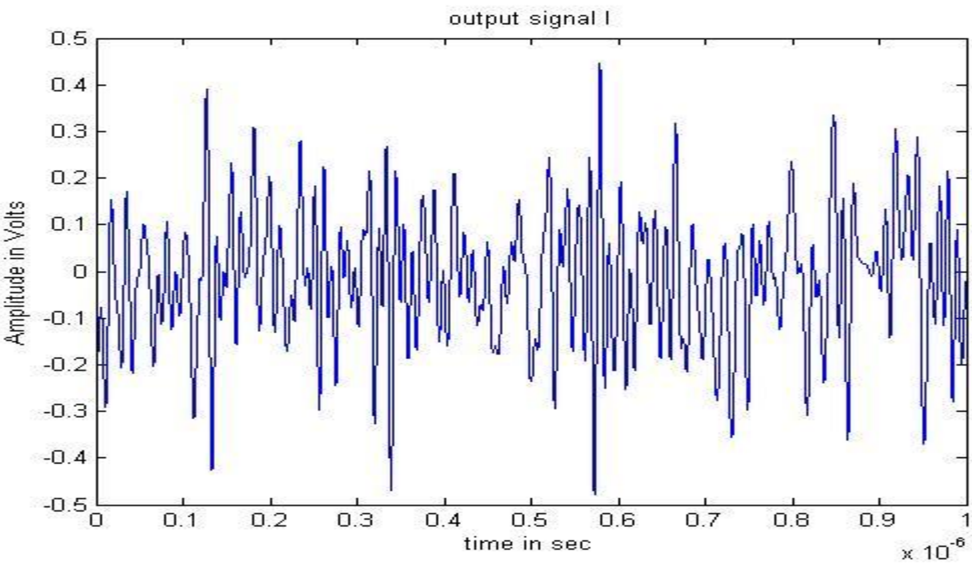

Figure 5.14 LPF output signal

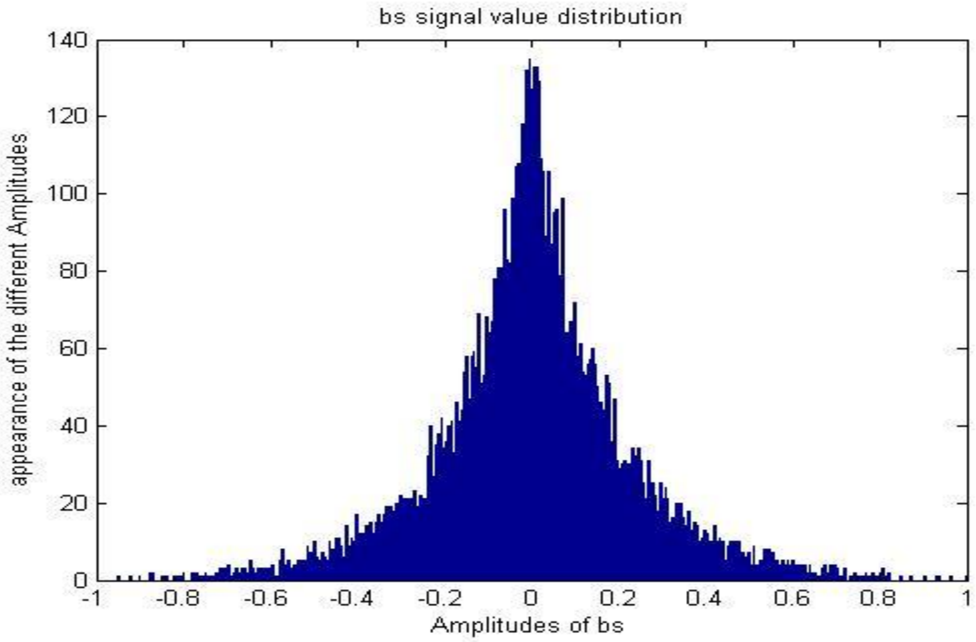

Figure 5.15 $b_{s\_noise}(t)$ value distribution

Applying the FFT to the simulated LPF output $b_{s\_noise}(t)$ results in a complex frequency spectrum $B_{s\_noise}(f)$. Both the real and imaginary components of $B_{s\_noise}(f)$ are zero mean Gaussian processes with equal standard deviations. Figure 5.16 depicts the real component of the frequency spectrum and figure 5.17 depicts the corresponding Gaussian distribution. The Matlab operation 'Lillietest' is performed on the real component of $B_{s\_noise}(f)$ and confirms that it is zero mean Gaussian distributed. Figure 5.18 depicts the imaginary component of the frequency spectrum and figure 5.19 depicts the corresponding Gaussian distribution. The Matlab operation 'Lillietest' is performed on the imaginary component of $B_{s\_noise}(f)$ and confirms that it is zero mean Gaussian distributed.

The analysis has shown that $|B_{s\_noise}(f)|$ is a Rayleigh distribution process. This is verified and validated by computing the magnitude of $B_{s\_noise}(f)$. Figure 5.20 depicts the Rayleigh distribution of $B_{s\_noise}(f)$.

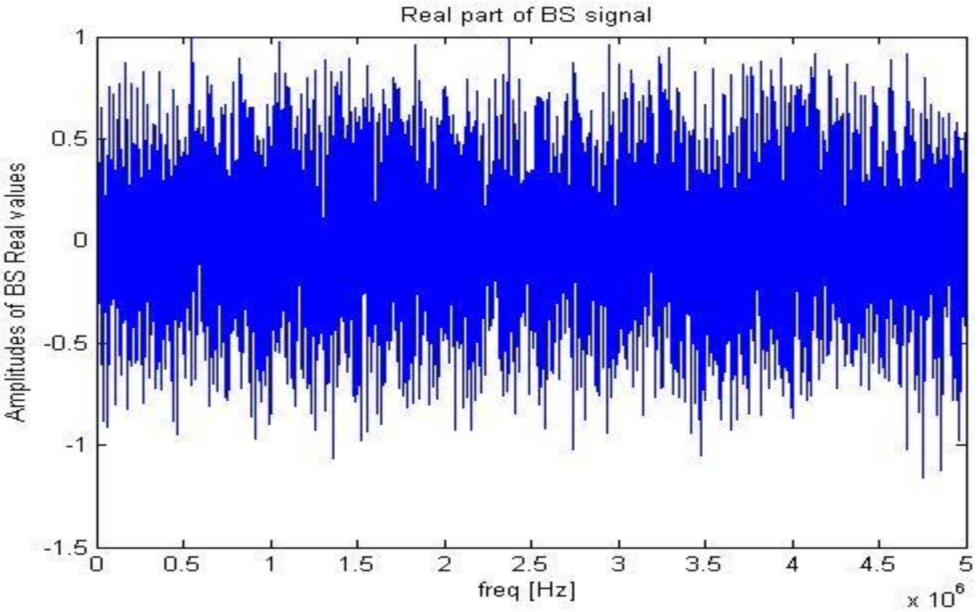

Figure 5.16 Frequency spectrum of real part of $B_{s\_noise}(f)$

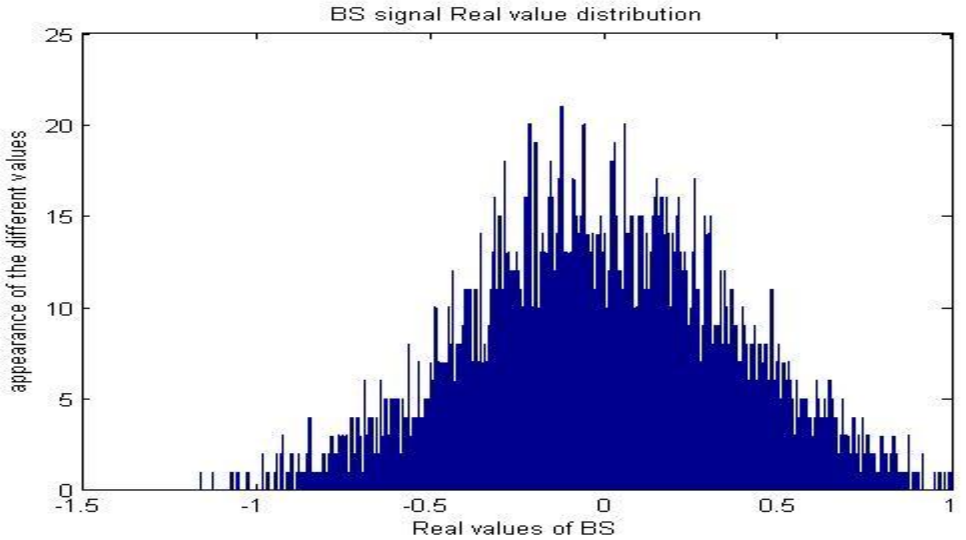

Figure 5.17 Amplitude distribution of the real part of $B_{s\_noise}(f)$

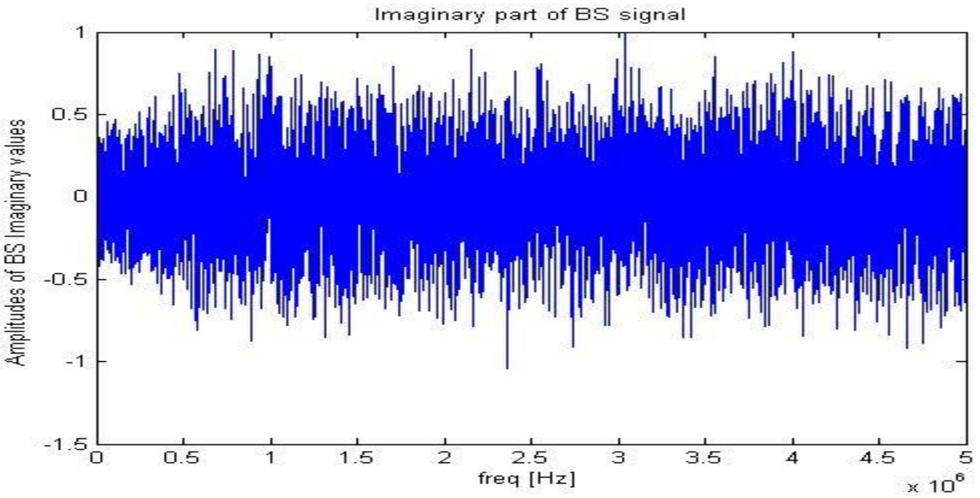

Figure 5.18 Frequency spectrum of imaginary part of $B_{s\_noise}(f)$

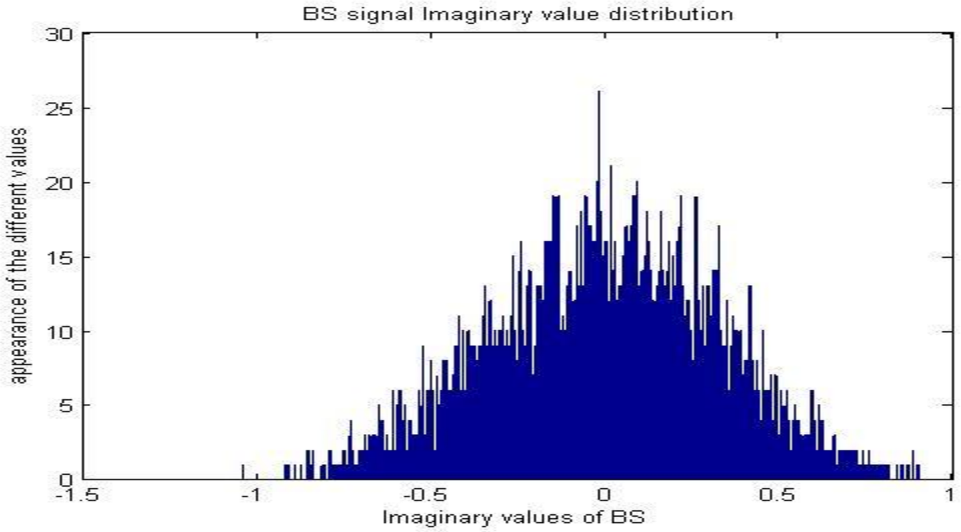

Figure 5.19 Amplitude distribution of the imaginary part of $B_{s\_noise}(f)$

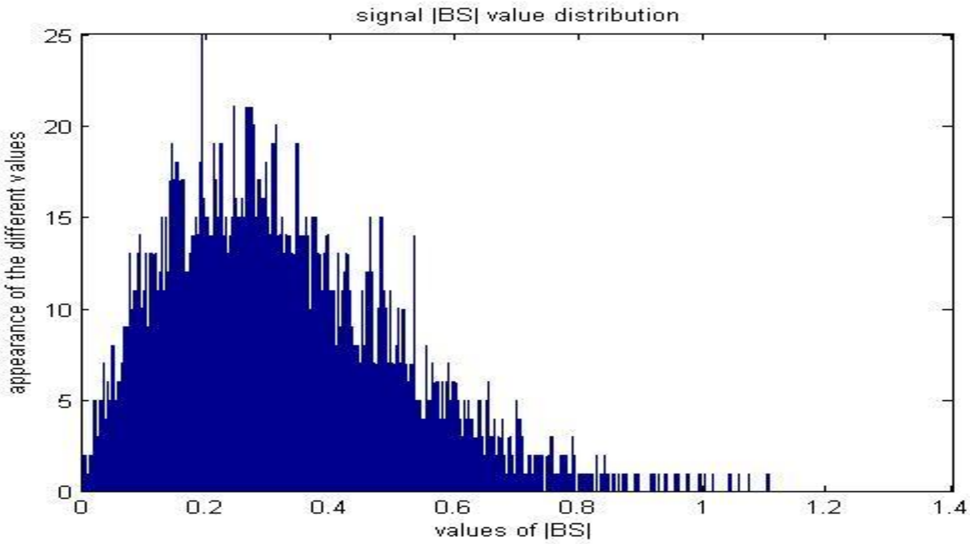

Figure 5.20 Magnitude distribution of $\left|B_{s\_noise}(f)\right|$

5.4.4 Range Error Deviation versus Signal to Noise Ratio

This paragraph shows the simulation results for the range error deviation versus the signal to noise ratio. Before showing the relation between the range error deviation and the *SNR*, the parameters used to conduct this simulation are explained.

For the simulation, a noise sample is generated with a bandwidth of 1GHz and a unit variance. For Matlab to show/plot a 1GHz bandwidth of a signal, the sample frequency must be twice the maximum frequency of the bandwidth. The sample frequency is a relation between the number of used samples and the duration of the observed signal. This relation is given by:

$$f_{sample} = 2f_{\max} = \frac{N}{T_{observed}} \tag{5.60}$$

Thus, $f_{sample} = 2f_{\max} = 2\text{GHz}$. The duration of the observed signal is chosen to be $T_{observed} = 10\mu s$. This results in a number of samples per observed time of $N = 20000$. For conducting the simulations, this *N* results in an acceptable simulation process time.

The received FMCW signal has a time delay of $\tau_d = 0.25\mu s$. This time delay is chosen because it is within the observed signal time and, according to eq. (4.14) and (4.15), this time delay results respectively in a beat frequency of $f_b = 250\text{KHz}$ and in a maximum range of $R = 75\text{m}$.

This FMCW signal and noise process is applied to the (simulated) receiver process. The Matlab FFT operation transforms the time signal into a frequency representation with a frequency resolution of $1/T_{observed} = 100\text{KHz}$. This does not provide a very accurate beat frequency. When no additional parameters are given for the FFT operation, it uses the number of samples of the provided time signal to produce the corresponding frequency components of its frequency spectrum. By using a higher number of samples for the FFT operation, the same frequency spectrum is divided in more frequency components. This results in an increased frequency resolution. Notice that the amplitude values corresponding to these extra frequency components (between two measurements) are interpolations. A drawback of this solution is, when the number of samples (the FFT operation has to process) increases too much, the simulation process time increases too, leading to unacceptable simulation process times. Another way to increase the frequency resolution is to increase the observation time. The drawback of this solution is that *N* increases also in order to maintain the 1GHz bandwidth. This also leads to unacceptable simulation process times. In this simulation a frequency resolution is created of 1KHz via the FFT solution by performing the FFT operation where the number of samples is multiplied with a factor 100.

As described in paragraph 5.3.5, two CRLB's are introduced. The CRLB based on time estimation and the CRLB based on frequency estimation. Figure 5.21 depicts the simulated range error deviation versus the signal to noise ratio and both CRLB's, based on a frequency resolution of 1KHz.

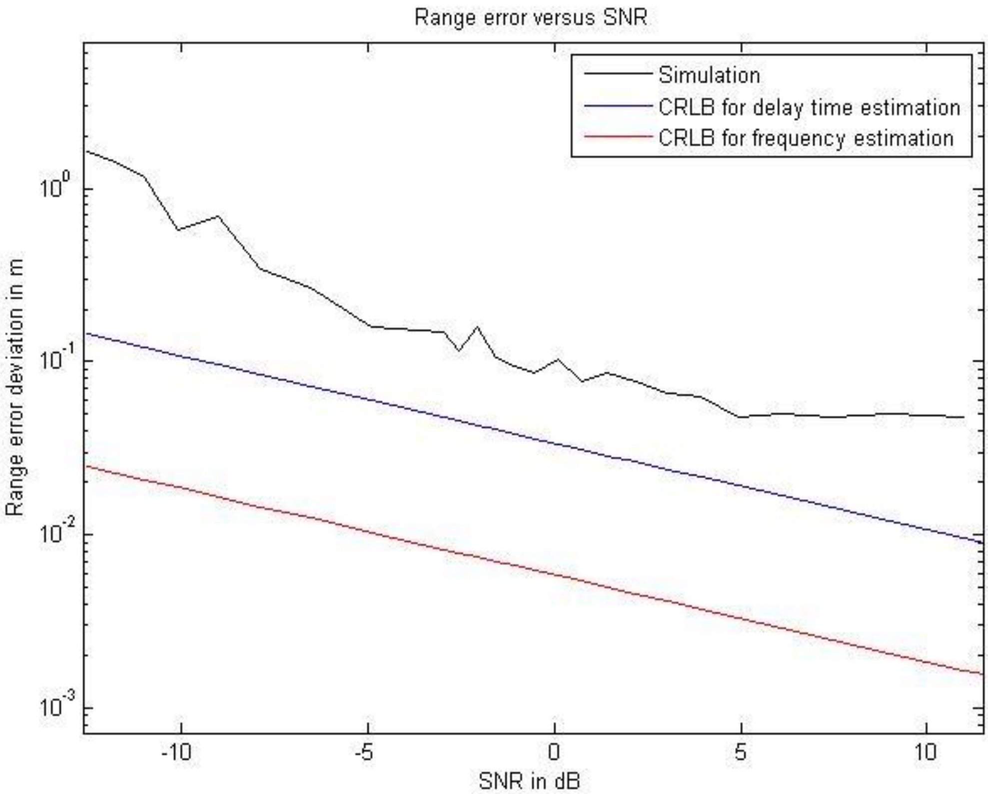

Figure 5.21 Range Error Deviation versus Signal to Noise Ratio

Figure 5.21 can be divided into four different parts. The first part, until -7 dB, shows the range error deviation for small SNR's. Here the simulation shows large deviations which corresponds to the theory which shows that for small SNR's the CRLB is not valid any more. The second part, from -7 dB till 5 dB, is where the simulated range error deviation approximate the CRLB. For the third part, from 5 dB till 12 dB, the simulated range error deviation is constant. This is due to the fact that the simulation process cannot produce more accurate calculations. The last part, from 12 dB and further (which is not shown in figure 5.21), is the part where the simulation is zero (for very high SNR's). The beat frequency errors (noise corrupted estimated beat frequency minus noise free original beat frequency) are zero.

For high enough SNR values, the simulation shows that range errors in the order of centimeters can be achieved. Therefore, this simulation shows that ranging based on FMCW signals is an accurate ranging method.

5.5 Summary

In the receiving process, the noise and the FMCW signal can be treated as independent signals and thus can be processed separately. Therefore, for the noise analysis, only the noise as input signal is considered.

The ACF based noise analysis shows that the sampled LPF output noise signal is a stationary process. Statistically characterizing this signal shows that it can be described as zero mean Gaussian. The FFT of this noise process results in a complex valued frequency spectrum. Both real and imaginary part of this noise process' frequency spectrum are zero mean jointly Gaussian. In case of only noise, the magnitude of this complex frequency spectrum is a Rayleigh process. For a FMCW signal in the presence of noise, the magnitude of this complex frequency spectrum is a Rician process.

The maximum range the system can cover, depends on the minimum required SNR (at the LPF output). For the UWB FMCW system (with parameters given by Table 5.1) the maximum range is $R \leq 278$ m. An UWB pulse based ranging system with the same input parameters, results in a maximum range value of $R \leq 128$ m. For the UWB FMCW ranging system, the large average transmit power and the substantial amount of energy received, positively affects the ranging performance.

Errors occur when estimating the beat frequency from the noise corrupted UWB FMCW receiver output. The CRLB provides the theoretical minimum range error variance. Equations (5.58) and (5.59) show that the minimum range error deviation is inversely proportional to the SNR and bandwidth of the signal. Simulations show that for high enough SNR's, range errors are in the order of centimeters. This means that ranging based on UWB FMCW technique is very promising for indoor ranging applications.

Conclusions and Future Work 6

This Chapter discusses the conclusions of the study on the influence of noise on ranging with FMCW signals and future work what needs to be done in order to complete the research of the behavior of this UWB FMCW Ranging system in the presence of noise.

6.1 Conclusions

The noise analysis of the UWB FMCW receiver is conducted based on the ACF of the receiver output. Because the FMCW signal and the noise are independent signals, the noise process can be treated separately. When only noise is present at the input of the FMCW receiver, the receiver's FFT output (the frequency spectrum of the beat signal) is a complex valued stationary noise process (consisting of two orthogonal zero mean jointly Gaussian processes with equal standard deviation).

The maximum range of the UWB FMCW receiver system is proportional to the bandwidth of the UWB FMCW signal and inversely proportional to the SNR. According to the FCC power regulations for FMCW signals, the larger the bandwidth the higher the average transmitted power. For an UWB FMCW system (with parameters given by Table 5.1), a maximum range is calculated of $R \leq 278\,\text{m}$. When these parameters are applied to an UWB pulse based ranging system, it shows a maximum range of $R \leq 128\,\text{m}$. Based on the same system parameter values, the UWB FMCW ranging system transmit more energy than an UWB pulse based ranging system which translates into a higher maximum range.

The presence of noise alters the UWB FMCW frequency spectrum. From this noisy signal the beat frequency is estimated. The presence of noise causes frequency estimation errors to occur which lead to range errors. The CRLB is introduced to provide a theoretical minimum range error deviation. This CRLB is inversely proportional to the SNR and the bandwidth of the signal.

Simulation of the range error deviation versus the SNR shows that for small SNR values, the CRLB is not valid any more. For high enough SNR values, the range error deviation is close to the CRLB. For higher SNR values the range error deviation shows to be constant, due to the limitations of the accuracy of the simulation process. For even higher SNR values no proper measurements can be done resulting in a range error deviation of zero. Depending on high enough SNR values, simulations shows that range errors in the order of centimeters can be achieved. Therefore, this simulation shows that ranging based on FMCW signal is an accurate ranging method.

6.2 Future Work

In this research some important assumptions were made. With these assumptions, some simplifications were made for the UWB FMCW ranging system in order to investigate the theoretical behavior of the system. These simplifications do not change the way the UWB FMCW ranging system operates. This paragraph sums these important assumption and shows what (future) work needs to be done to complete the analysis of UWB FMCW ranging system.

Analyze and validate the distribution model of the frequency spectrum of the noise corrupted process

In the analysis of the statistical characterization of the frequency spectrum of a noise corrupted process, no test bed situation is used to conduct real measurements.

Future work: Perform real measurements to validate the analysis and simulation results and present a distribution model for the deviation of estimated beat frequency related to certain signal to noise ratio. The standard deviation corresponding to that distribution model is proportional to the range variance.

Non linearity of frequency sweep.

Ranging by use of FMCW is based on a linear frequency sweep.

Assumption made in this report: Here, we assume that the transmitter produces an UWB FMCW signal which has a linear frequency sweep and that the replica of the transmitted signal (produced by the receiver system) has exactly the same linear frequency sweep.

Future Work: Future research must concentrate on how to produce an accurate linear frequency sweep and how to handle non-linearity in the frequency sweep. Non-linearity causes the beat signal to be a non single tone signal any more. This results in beat frequency estimation errors and eventually in range errors and decrease of accuracy of the UWB FMCW ranging system.

Narrow Band Interference.

With the explanation of the principles of UWB FMCW ranging, we assume the receiver system receives only one transmitted UWB FMCW signal. This signal is free of any interference, however, the presence of NBI (Narrow Band Interference) sources is very likely in a dense frequency spectrum.

Assumption made in this report: No external interference sources are present which could influence the ranging.

Future Work: Future research must explain the effect of NBI (Narrow Band Interference) on ranging. The actual influence of NBI on ranging must be investigated and how to minimize and/or avoid NBI on UWB FMCW ranging.

Multiple Access.

A ranging system is considered where one ranging device (of unknown location) transmits a UWB FMCW signal.

Assumption made in this report: Only one ranging device is considered to operate within the indoor environment.

Future Work: In case of more ranging devices, multiple UWB FMCW signals are received. These signals should be distinguishable, non-interfering with each other and separately processed by the receiver system. This increases the complexity and the computational intensity. Future research should explain how to distinguish and process the received signals from the multiple objects of interest, which operate within the same area (Multiple Access).

Appendix A Autocorrelation Function of $r(t)$

In this appendix, equation (5.21) is derived.

$$\begin{aligned}
R_r(t_1,t_2) &= E[r(t_1)r(t_2)], \\
&= E[(\sum_{n=1}^{N} a_n s(t-\tau_n) + (n(t)\otimes h_{BPF}(t)))(\sum_{n=1}^{N} a_n s(t+\tau-\tau_n) + (n(t+\tau)\otimes h_{BPF}(t+\tau))) \\
&= E[(\sum_{n=1}^{N} a_n s(t-\tau_n))(\sum_{n=1}^{N} a_n s(t+\tau-\tau_n)) + (\sum_{n=1}^{N} a_n s(t-\tau_n))(n(t+\tau)\otimes h_{BPF}(t+\tau)) + \\
&\quad (\sum_{n=1}^{N} a_n s(t+\tau-\tau_n))(n(t)\otimes h_{BPF}(t)) + (n(t)\otimes h_{BPF}(t))(n(t+\tau)\otimes h_{BPF}(t+\tau))]
\end{aligned} \tag{A-1}$$

$$\begin{aligned}
&= E[(\sum_{n=1}^{N} a_n s(t-\tau_n))(\sum_{n=1}^{N} a_n s(t+\tau-\tau_n))] + E[(\sum_{n=1}^{N} a_n s(t-\tau_n))(n(t+\tau)\otimes h_{BPF}(t+\tau))] + \\
&\quad E[(\sum_{n=1}^{N} a_n s(t+\tau-\tau_n))(n(t)\otimes h_{BPF}(t))] + E[(n(t)\otimes h_{BPF}(t))(n(t+\tau)\otimes h_{BPF}(t+\tau))]
\end{aligned}$$

From this formula the expectation operation is applied to the process and the deterministic part is placed out site the expectation brackets. This results in:

$$\begin{aligned}
R_r(t_1,t_2) &= E[(\sum_{n=1}^{N} a_n s(t-\tau_n))(\sum_{n=1}^{N} a_n s(t+\tau-\tau_n))] + E[n(t+\tau)\otimes h_{BPF}(t+\tau)]\sum_{n=1}^{N} a_n s(t-\tau_n) + \\
&\quad E[n(t)\otimes h_{BPF}(t)]\sum_{n=1}^{N} a_n s(t+\tau-\tau_n) + E[(n(t)\otimes h_{BPF}(t))(n(t+\tau)\otimes h_{BPF}(t+\tau))]
\end{aligned} \tag{A-2}$$

Before continuing this calculation, the part describing the convolution between the stationary zero mean Gaussian process $n(t)$ and the impulse response of the BPF $h_{BPF}(t)$ is treated.

$$\begin{aligned}
E[n(t)\otimes h_{BPF}(t)] &= E[\int_{-\infty}^{\infty} n(t+\tau)h_{BPF}(\tau)d\tau] \\
&= \int_{-\infty}^{\infty} E[n(t+\tau)]h_{BPF}(\tau)d\tau \\
&= \int_{-\infty}^{\infty} \mu_n(t)h_{BPF}(\tau)d\tau \\
&= \mu_n(t)\int_{-\infty}^{\infty} h_{BPF}(\tau)d\tau
\end{aligned} \tag{A-3}$$

where $\mu_n(t)$ is the mean of the stationary noise process which is zero. This results in (A-3) to be zero.

Applying this to (A-2) indicates that the second and third term are zero. Now, (A-2) is written as:

$$R_r(t_1,t_2) = E[(\sum_{n=1}^{N} a_n s(t-\tau_n))(\sum_{n=1}^{N} a_n s(t+\tau-\tau_n))] + E[n(t)n(t+\tau)]\otimes h_{BPF}(t)\otimes h_{BPF}(t+\tau) \tag{A-4}$$

Treating only the (second) noise part of the summation, shows that (A-4) can be written as:

$$
\begin{aligned}
E[n(t)\otimes h_{BPF}(t)n(t+\tau)\otimes h_{BPF}(t+\tau)] &= E[\int_{-\infty}^{\infty} n(t-u)h_{BPF}(u)du \int_{-\infty}^{\infty} n(t+\tau-v)h_{BPF}(v)dv] \\
&= E[\int_{-\infty}^{\infty}\int_{-\infty}^{\infty} n(t-u)h_{BPF}(u)n(t+\tau-v)h_{BPF}(v)dudv] \\
&= \int_{-\infty}^{\infty}\int_{-\infty}^{\infty} E[n(t-u)n(t+\tau-v)]h_{BPF}(u)h_{BPF}(v)dudv \\
&= \int_{-\infty}^{\infty}\int_{-\infty}^{\infty} E[n(t)n(t+\tau-v+u)]h_{BPF}(u)h_{BPF}(v)dudv \\
&= \int_{-\infty}^{\infty}\int_{-\infty}^{\infty} R_n(t,t+\tau-v+u)h_{BPF}(u)h_{BPF}(v)dudv
\end{aligned}
\qquad \text{(A-5)}
$$

Because $n(t)$ is a stationary process (A-5) can be written as:

$$
\begin{aligned}
E[n(t)\otimes h_{BPF}(t)n(t+\tau)\otimes h_{BPF}(t+\tau)] &= \int_{-\infty}^{\infty}\int_{-\infty}^{\infty} R_n(\tau-v+u)h_{BPF}(u)h_{BPF}(v)dudv \\
&= \int_{-\infty}^{\infty} h_{BPF}(u)\{\int_{-\infty}^{\infty} R_n((\tau+u)-v)h_{BPF}(v)dv\}du \\
&= \int_{-\infty}^{\infty} h_{BPF}(u)\{h_{BPF}(\tau+u)\otimes R_n(\tau+u)\}du \\
&= \int_{-\infty}^{\infty} h_{BPF}(u)\{h_{BPF}(-((-\tau)-u))\otimes R_n(-((-\tau)-u))\}du \\
&= h_{BPF}(-\tau)\otimes h_{BPF}(\tau)\otimes R_n(\tau)
\end{aligned}
\qquad \text{(A-6)}
$$

Applying (A-6) to (A-4) results in equation (5.20). This is given by:

$$
R_r(t_1,t_2) = E[(\sum_{n=1}^{N} a_n s(t-\tau_n))(\sum_{n=1}^{N} a_n s(t+\tau-\tau_n))] + R_n(\tau)\otimes h_{BPF}(\tau)\otimes h_{BPF}(-\tau) \qquad \text{(A-7)}
$$

Appendix B Performance Gain

The calculation of the G_{SNR} is split into two parts. First the (double sided spectrum) signal power at the BPF output and at the LPF output are discussed. After that, the (double sided spectrum) noise power at the BPF output and at the LPF output are discussed. The signal to noise ratio at the BPF output and at the LPF output are indicated as SNR_{BPF} and SNR_{LPF}, respectively.

Without the presence of noise, the received power at the BPF output is addressed as P_q.

$$\begin{aligned} P_q &= \overline{(s(t+\tau_d))^2} = \overline{\cos^2 2\pi(f_l(t+\tau_d)+\tfrac{1}{2}\zeta(t+\tau_d)^2)} \\ &= \overline{\tfrac{1}{2}+\tfrac{1}{2}\cos 2\pi 2(f_l(t+\tau_d)+\tfrac{1}{2}\zeta(t+\tau_d)^2)} = \tfrac{1}{2}[W] \end{aligned} \quad \text{(C-1)}$$

The reference signal $s'(t)$ is given by;

$$s'(t) = 2\cos 2\pi(f_l t + \tfrac{1}{2}\zeta t^2) \quad \text{(C-2)}$$

The mixed signal $z(t)$ is given by;

$$\begin{aligned} z(t) &= s(t+\tau_d)s'(t) = (\cos 2\pi(f_l(t+\tau_d)+\tfrac{1}{2}\zeta(t+\tau_d)^2)2\cos 2\pi(f_l t+\tfrac{1}{2}\zeta t^2))^2 \\ &= \cos 2\pi(f_l\tau_d+\zeta t\tau_d+\tfrac{1}{2}\zeta\tau_d^2)+\cos 2\pi(2f_l t+f_l\tau_d+\zeta t^2+\zeta t\tau_d+\tfrac{1}{2}\zeta\tau_d^2) \end{aligned} \quad \text{(C-3)}$$

The LPF filtered signal $b_s(t)$ is given by;

$$b_s(t) = \cos 2\pi(f_l\tau_d+\zeta t\tau_d+\tfrac{1}{2}\zeta\tau_d^2) \quad \text{(C-4)}$$

The power of $b_s(t)$ is given by;

$$\begin{aligned} P_{b_s} &= \overline{(\cos 2\pi(f_l\tau_d+\zeta t\tau_d+\tfrac{1}{2}\zeta\tau_d^2))^2} \\ &= \overline{\tfrac{1}{2}+\tfrac{1}{2}\cos 2\pi 2(f_l\tau_d+\zeta t\tau_d+\tfrac{1}{2}\zeta\tau_d^2)} = \tfrac{1}{2}[W] \end{aligned} \quad \text{(C-5)}$$

The available noise power depends on the bandwidth of the signal. The noise power at the BPF output is given by:

$$\begin{aligned} P_{q_n} &= \overline{n^2(t)} = \overline{(n_x(t)\cos\omega_c t - n_y(t)\sin\omega_c t)^2} = \\ &\tfrac{1}{2}\overline{(n_x^2(t)+n_y^2(t))} = \sigma_n^2 \end{aligned} \quad \text{(C-6)}$$

The noise process at the mixer output is given by:

$$\begin{aligned} z_n(t) &= ((n_x(t)\cos\omega_c t - n_y(t)\sin\omega_c t))2\cos 2\pi(f_l t+\tfrac{1}{2}\zeta t^2)) = \\ &= 2[(\tfrac{1}{2}n_x(t)\cos 2\pi(W_b t-\tfrac{1}{2}\zeta t^2)-\tfrac{1}{2}n_y(t)\sin 2\pi(W_b t-\tfrac{1}{2}\zeta t^2))+ \\ &\quad (\tfrac{1}{2}n_x(t)\cos 2\pi(2f_l t+W_b t+\tfrac{1}{2}\zeta t^2)-\tfrac{1}{2}n_y(t)\sin 2\pi(2f_l t+W_b t+\tfrac{1}{2}\zeta t^2))] \end{aligned} \quad \text{(C-7)}$$

(C-7) consists of a baseband and a bandpass component.

The (single sided) noise power at the mixer output is also given as;

$$P_{z_n} = \int_0^{B_{BPF}} PSD_{z_n} df \tag{C-8}$$

The power of the baseband component of $z_n(t)$ is given by;

$$\begin{aligned} P_{z_n baseband} &= \overline{(n_x(t)\cos 2\pi(W_b t - ½\zeta t^2) - n_y(t)\sin 2\pi(W_b t - ½\zeta t^2))^2} \\ &= ½\,\overline{(n_x^2(t) + n_y^2(t))} = \sigma_n^2 \end{aligned} \tag{C-9}$$

The LPF allows only the baseband component of $z_n(t)$ to pass of which the frequencies are limited by the cut-off frequency of the LPF. Therefore, LPF 'selects' only a small part of the baseband noise of $z_n(t)$.

$$P_{b_n} = \int_0^{B_{LPF}} PSD_{z_n baseband} df \tag{C-10}$$

P_{b_n} is given by:

$$P_{b_n} = \frac{B_{LPF}}{B_{BPF}} P_{z_n baseband} = \frac{B_{LPF}}{B_{BPF}} \sigma_n^2 = \frac{B_{LPF}}{B_{BPF}} P_{q_n} \tag{C-11}$$

For B_{LPF} is 5Mhz and the B_{BPF} is 1 GHz, the ratio between SNR_{LPF} and SNR_{BPF} is given by:

$$G_{snr} = \frac{SNR_{LPF}}{SNR_{BPF}} = \frac{\dfrac{P_{b_s}}{P_{b_n}}}{\dfrac{\mathrm{P}_q}{P_{q_n}}} = \frac{P_{b_s}}{P_{b_n}} \frac{P_{q_n}}{\mathrm{P}_q} = \frac{½}{\dfrac{B_{LPF}}{B_{BPF}} P_{q_n}} \frac{P_{q_n}}{½} = \frac{B_{BPF}}{B_{LPF}} = 200 \tag{C-12}$$

References

[1] www.sensorwiki.org

[2] http://www.kowoma.de/en/gps/accuracy.htm, subject 'The GPS System, Achievable Accuracy'.

[3] www.gisdevelopment.net

[4] FCC, Office of Engineering and Technology, *"Revision of part 15 of the commission's rules regarding ultra-wideband transmission systems"*, ET Docket, no. 98-153, 2002.

[5] H. Nikookar, R. Prasad, '*Introductions to Ultra WideBand for Wireless Communications*', Springer 2009.

[6] M. Ghavami, L. B. Micheal, R. Kohno, '*Ultra Wideband signals and systems in communication engineering*', Wiley, 2007

[7] http://www.radartutorial.eu/01.basics/rb07.en.html

[8] B. Mullarkey, Technical briefing '*The Difference between Pulse Radars and FMCW Onces*', for www.navigate-us.com, December 2008.

[9] A. G. Stove, *'Linear FMCW radar techniques'*, IEE-Proceedings-F, Vol. 139, No.5, October 1992.

[10] A. F. Molisch, D. Cassioli, C. Chong, S. Emami, A. Fort, B. Kannan, J. Karedal, J. Kunisch, H. Schantz, K. Siwiak, M. Win, '*A Comprehensive Standardized Model for Ultrawideband Propagation Channels'*, IEEE, vol. 54, No. 11, November 2006.

[11] A. F. Molisch, *'Ultrawideband Propagation Channels-Theory Measurement, and Modeling'*, Invited Paper, IEEE, vol. 54, No. 5, pp 1528-1545, September 2005.

[12] A. Goldsmith, *'Wireless Communication'*, Cambridge University Press, 2005

[13] A. Muqaibel, A. Safaai-Jazi, A. Bayram, A. M. Attiya and S. M. Riad, '*Ultrawideband through-the-wall propagation*', IEEE, vol 152, No. 6, pp 581-588, December 2005

[14] A. F. Molisch, K.Balakrishnan, D. Cassioli, C. Chong, S. Emami, A. Fort, J. Karedal, J. Kunisch, H. Schantz, K. Siwiak, '*A Comprehensive Model for Ultrawideband Propagation Channels*', IEEE GLOBECOM 2005, vol 6, pp. 3648-3653, 28 November – 2 December 2005.

[15] http://en.wikipedia.org/wiki/Nakagami_distribution

[16] H. Nikookar, Lecture notes '*Advanced topics in Digital Wireless Communications*', IRCTR- Delft University of technology, 2004.

[17] G. M. Brooker, '*Understanding Millimeter Wave FMCW Radars*', 1st International Conference on Sensing technology New Zealand, November 2005.

[18] L. Barclay, *'Propagation of Radiowaves'*, IEE, 2003

[19] Bernard Sklar, '*Digital Communications Fundamentals and Applications*', Prentice Hall 1988

[20] L. W. Couch II, '*Digital and Analog Communication Systems'*, Prentice Hall 2001.

[21] R. D. Yates, D. J. Goodman, '*Probability and Stochastic Processes'*, Wiley 2004.

[22] K. F. Riley, M P. Hobson and S. J. Bence, '*Mathematical Methods for Physics and Engineering*', Cambridge University Press 2006, Chapter 13, pp 436.

[23] Amitabha Bhattacharya, '*Digital Communications*', Tata McGraw-Hill 2006

[24] Webpage Bores Signal Processing, *http://www.bores.com/courses/advanced/windows/10_cpg.htm*

[25] Hamish Meikle, 'Modern Radar Systems', ARTECH HOUSE INC, 2001.

[26] F. Harris, '*On the Use of Windows for Harmonic Analysis with the Discrete Fourier Transform*' , Proceedings of the IEEE, Vol. 66, no. 1, pp. 51-83, January 1978.

[27] C. Liao, S. Liu, '*A Broadband Noise-Canceling CMOS LNA for 3.1-10.6 GHz UWB Receivers*', IEEE Journal of Solid-State Circuits, Vol. 42, No. 2, pp. 329-339. February 2007.

[28] P. Sun, S. Liao, H. Lin, C. Yang, Y, Hsiao, '*Design of 3.1 to 10.6 GHz Ultra-wideband Low Noise Amplifier with Current Reuse Techniques and Low Power Consumption*', Progress In Electromagnetics research Symposium, Beijing, China, March 23-27, 2009, pp 901-905

[29] F. Lee, A Chandrakasan, *'A BiCMOS Ultra-Wideband 3.1-10.6 GHz Front-end*', IEEE Journal of Solid-State Circuits, Vol. 41, no. 8, pp 1784-1791, August 2006.

[30] Robert J. Fontana, Edward A. Richley, *"Observations on Low Data Rate, Short Pulse UWB Systems"*, IEEE ICUWB 200, pp 334-338, Sep. 2007

[31] S. Gezici, Zhi Tian, G. B. Giannakis, H. Kobayashi, A. F. Molisch, H. V. Poor, Z. Sahinoglu, '*Localization via ultra-wideband radios: a look at positioning aspects for future networks*', Signal Processing Magazine IEEE, Vol. 22, no. 4, pp. 70-84, July 2005.

[32] Gai, Jing Chan, Francois Chan, Y.T. Du, Huai-Jing Dilkes, Fred A, '*Frequency Estimation of Uncooperative Coherent Pulse Radars*', Military Communications Conference 2007, MILCOM 2007 IEEE, 29-31 October 2007 pp 1-7.

[33] D. Rife, R. Boorstyn, '*Single-Tone Parameter Estimation from Discrete-Time Observations*', IEEE Transactions on Information Theory, Vol. 20, no. 5, pp. 591-598, September 1974.

[34] S. Tretter, '*Estimating the Frequency of a Noisy Sinusoid by Linear Regression*', IEEE Transactions on Information Theory, Vol. 31, no.6, pp.832-835, November 1985.

[35] S. Kay, '*A Fast and Accurate Single Frequency Estimator*', IEEE Transactions on Acoustic Speech and Signal Processing, Vol. 37, no. 12, pp.1987-1990, December 1987.